Analyses of MPPT algorithms in real test conditions

THIAGO FIALHO GUIMARÃES

Supervised by

Prof. Dr. Américo Vicente Teixeira Leite

Prof. Dr. Alceu André Badin

Bragança

2019-2020

Analyses of MPPT algorithms in real test conditions

THIAGO FIALHO GUIMARÃES

Thesis presented in the School of Technology and Management of the Polytechnic Institute of Bragança to fulfill the requirements of a Master of Science Degree in Industrial Engineering (Electrical Engineering branch).

Supervised by

Prof. Dr. Américo Vicente Teixeira Leite

Prof. Dr. Alceu André Badin

Bragança

2019-2020

Acknowledgments

First of all, I would like to thank God, for my life, and for allowing me to overcome all the obstacles encountered in carrying out this work.

I would like to thank my advisor Dr. Américo Vicente Leite for the support, motivation, criticism and advice, which were of great help for the evolution as a person and student, and in addition, had a direct impact on the results achieved in this work. I would also like to thank Prof. Alceu André Badin, for accepting the invitation to be my mentor from UTFPR in Brazil.

I thank all my family, especially my mother, Hilda, my father Antonio and my brother Marcello, who always showed support, shared moments of difficulty, joy and made it possible to study in Portugal.

I am grateful to my girlfriend Cassia Liliane for the encouragement and support in the difficult times encountered during this work.

My thanks to Leonardo Biazote, a great friend, for helping whenever I needed it, helping me with the arrival and with preparation processes related to coming to Portugal.

I would like to thank my colleagues with whom I shared the IPB research laboratory: Alice Fey, Victor Polidorio, Victor Ávila, Henrique Quaresma, Marina Pietrobelli, Chellal Majd and Fabiano Peretti.

Finally, I would also like to thank the people not mentioned here who, directly or indirectly, contributed to the writing of this document.

Resumo

Os algoritmos de rastreamento do Ponto de Potência Máxima (MPPT) têm grande relevância para o rendimento otimizado em sistemas fotovoltaicos conectados à rede. Muitos algoritmos foram investigados. No entanto, existe uma grande dificuldade em encontrar análises comparativas com resultados experimentais entre as diferentes técnicas, já que grande parte das pesquisas se baseiam em revisões da literatura ou em simulação.

Este trabalho apresenta um análise experimental entre quatro técnicas MPPT, que estão entre as mais discutidas na literatura: duas das mais simples (Perturb & Observe e Condutância Incremental) e duas das mais complexas (Particle Swarm Optimization e Fuzzy Logic Controller). São utilizados ainda inversores comerciais disponíveis para teste em laboratório, com objetivo de entender qual algoritmo MPPT é utilizado, o seu funcionamento e procedimento de inicialização.

Todos os algoritmos são implementados e validados durante testes experimentais, sob condições reais, as quais operam os sistemas PV. Os testes buscam ainda garantir as mesmas condições experimentais, para que a avaliação de desempenho de cada algoritmo reflita o seu real desempenho em rastrear o ponto de máxima potência.

Os testes experimentais são divididos em 3: testes em condições normais, testes em condição de sombreamento parcial e testes com inversores PV comerciais.

Para a sua implementação, utilizou-se uma estrutura de potência baseada em um conversor DC-DC elevador ou conversor Boost, e um inversor monofásico de ponte completa. O controle e leitura dos sinais é implementado utilizando o Simulink® e dSPACE 1103, placa controladora em tempo real. Além disso, as técnicas MPPT de três inversores comerciais também são analisados.

Abstract

Maximum Power Point tracking algorithms (MPPT) have great relevance for the optimized performance in photovoltaic systems connected to the grid. Many algorithms have been investigated. However, there is a great difficulty in finding comparative analyzes based on experimental results between the different techniques, since most of the research is based on literature reviews or simulation.

This work presents an experimental analysis between four MPPT techniques, which are among the most discussed in the literature: two of the simplest (Perturb & Observe and Incremental Conductance) and two of the most complex (Particle Swarm Optimization and Fuzzy Logic Controller). Commercial inverters available for laboratory testing are also used in order to understand which MPPT algorithm is used, how does it work and how is it initialized.

All algorithms are implemented and validated during experimental tests, under real conditions, which operate the PV systems. The tests also seek to guarantee the same experimental conditions, so that the performance evaluation of each algorithm reflects its real performance in tracking the maximum power point.

The experimental tests are divided into 3: tests under normal conditions, tests under partial shading condition and tests with commercial PV inverters.

For implementation, a power structure based on a DC-DC Boost converter and a single-phase full-bridge inverter was used. The control and reading of the signals is implemented using Simulink® and dSPACE 1103 real-time controller board. In addition, three MPPT techniques of commercial inverters are also analyzed.

Contents

List of Tables

List of Figures

Acronyms

AC	Alternating Current
DC	Direct Current
ESTiG	Escola Superior de Tecnologia e Gestão
FLC	Fuzzy Logic Controller
GMPP	Global Maximum Power Point
IC	Icremental Condutance
IGBT	Insulated Gate Bipolar Transistor
IPB	Instituto Politécnico de Bragança
LSE	Laboratório de Sistemas Eletromecatrónicos
MPP	Maximum Power Point
MPPT	Maximum Power Point Tracking
PID	Proportional-Integral-Derivative Control
PLL	Phase Locked Loop
PO	Pertub and Observe
PSO	Particle Swarm Optimization
PV	Photovoltaic
VOC	Voltage Oriented Control

List of Symbols

	Description	Unit if applicable
V_{pv}	Voltage of photovoltaic string	Volts (V)
I_{pv}	Current of photovoltaic string	Ampere (A)
V_{mpp}	Voltage at maximum power point	Volts (V)
V_{mppt}	Voltage of the MPPT algorithm	Volts (V)
I_{mpp}	Current at maximum power point	Ampere (A)
V_{oc}	Open circuit voltage	Volts (V)
I_{sc}	Short circuit current	Ampere (A)
V_{ref}	Reference voltage	Volts (V)
I_{ref}	Reference current	Ampere (A)
I_{d}	Current direct component	Ampere (A)
I_{q}	Current quadrature component	Ampere (A)
V_{d}	Voltage direct component	Volts (V)
V_{q}	Voltage quadrature component	Volts (V)
I_{α}	Current Alpha component	Ampere (A)
I_{β}	Current Beta component	Ampere (A)
V_{α}	Voltage Alpha component	Volts (V)
V_{β}	Voltage Beta component	Volts (V)
K_{p}	Gain - Proportional Component (PI)	-
K_{i}	Gain - Integral Component (PI)	-

Chapter 1

Introduction

Concerns about the effects of air pollution, energy security and access to energy are growing. Moreover, volatile oil prices in recent years have intensified the search for alternative low-carbon technologies, such as renewables.

The generation of renewable sources has expanded faster than the generation of any other fuel. In Figure 1.1 it is possible to observe its growth over the last few years and the energy transition through which the world has been passing.

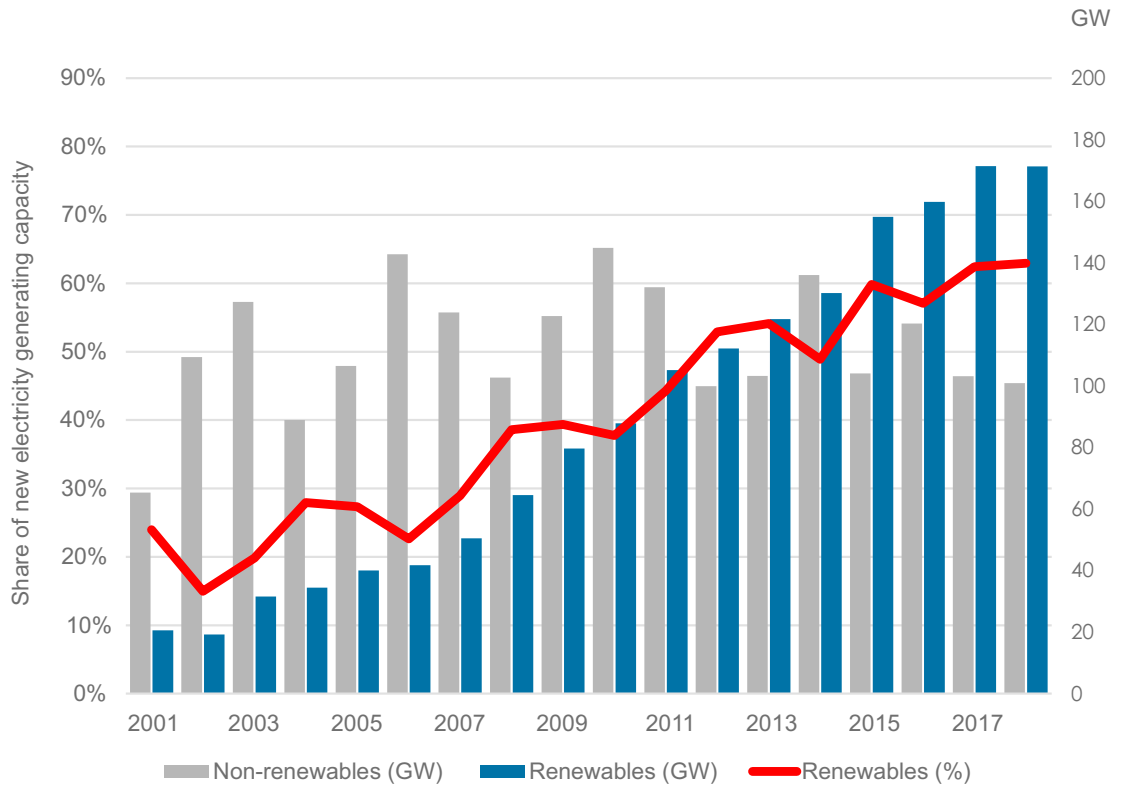

Figure 1.1: Renewable generation capacity and energy transition [1].

In 2019, renewable electricity generation increased by 6%, with solar photovoltaic and wind technologies, which together accounted for 64% of this growth. Photovoltaic solar

energy, on the other hand, had a generation increase of more than 22% from 2018 to 2019, thanks to continued support for cost reduction policies [2].

1.1 Photovoltaic Solar Energy

Photovoltaic energy has become increasingly known and used to generate electricity. It can be obtained from the direct conversion of sunlight, even on cloudy days, using photovoltaic cells. Today, it is one of the fastest growing renewable energy technologies and is ready to play an important role in the future global diversification of electricity generation [3].

Photovoltaic systems can be used to supply electricity on a large scale, for commercialization or even on small scales for individual consumption. The use of photovoltaic solar energy for individual consumption is an excellent way to provide access to people who do not live close to power transmission lines [3].

The installed capacity of solar photovoltaic energy in the world has grown considerably in recent years, reaching the 580 GW mark at the end of 2019, exceeding the number in 2010 by more than 10 times, as shown in Figure 1.2. These new additions to installed capacity were the highest among all renewable energy technologies for the year [1].

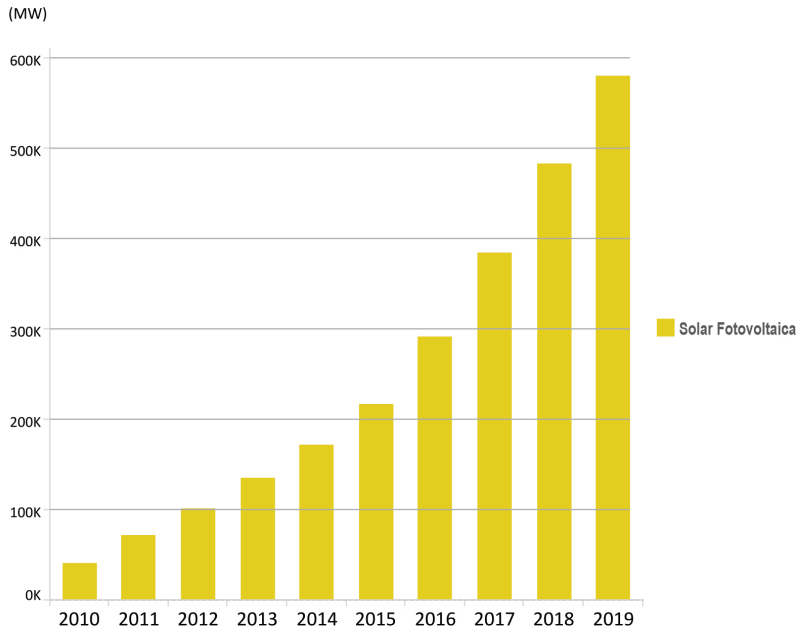

Figure 1.2: Photovoltaic energy capacity installed in recent years [4].

The cost trends of a photovoltaic system and its demand are important factors to improve the technology's competitiveness. Historically, the downward trend in system costs continued in 2019. Between December 2009 and December 2019, module prices fell and this weighted reduction in average cost may be in the order of 90% during this period [1].

The reason for a preference for solar energy over other technologies has been, among other reasons, its marked cost reduction curve that continues to decrease, as shown in Figure 1.3. The more efficient the system is, the lower the cost of the energy generated.

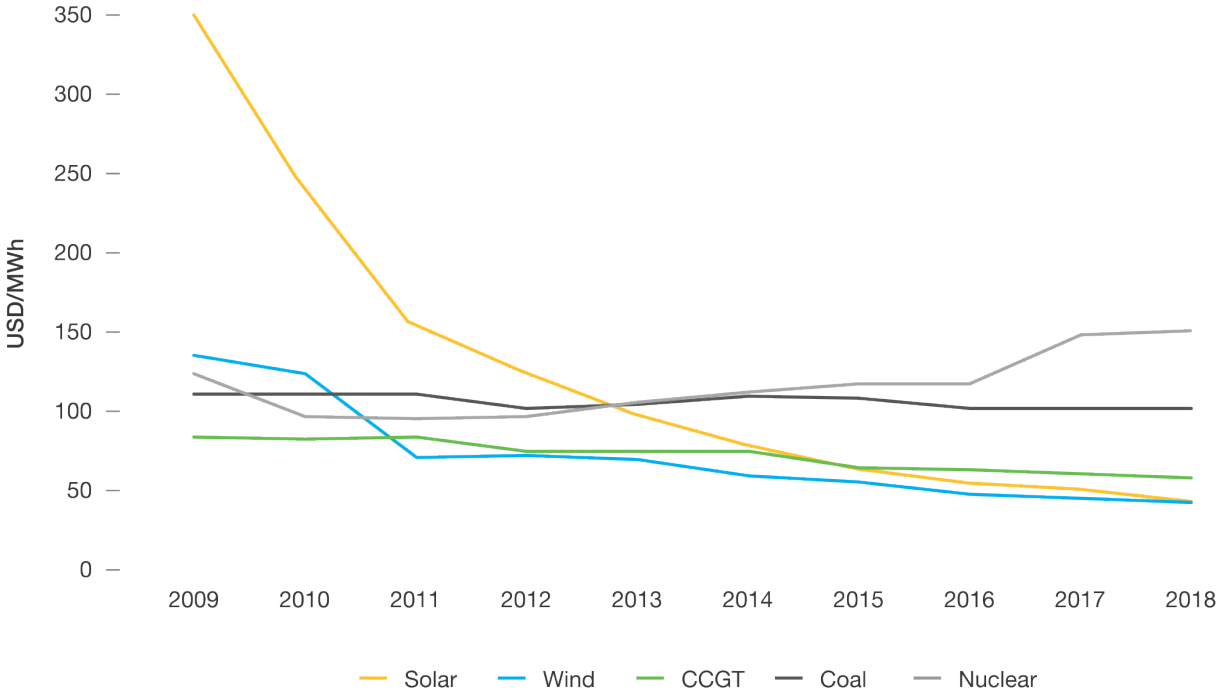

Figure 1.3: Cost of solar electricity generation compared to other sources [5].

1.2 Photovoltaic Systems

Photovoltaic systems can produce electricity without causing major environmental risks [6]. However, the wide acceptance, use and photovoltaic generation of electric energy are limited by the cost of production. Although this cost depends on the type of photovoltaic system used, it is also directly linked to its general efficiency and, with this, the delivery of greater energy [6].

A photovoltaic system, as shown in Figure 1.4, is composed of photovoltaic modules and energy conversion devices, such as photovoltaic inverters. Consequently, the solar cell is the basic element in the system, converting solar radiation into electricity. The system can also count on energy storage, to be available in the absence of solar radiation. In this case the energy produced by the PV string must be partially stored, usually using batteries. Electronic power circuits are also necessary to adapt, manage and distribute the generated energy. Equipment such as load controllers and inverters perform this function [7].

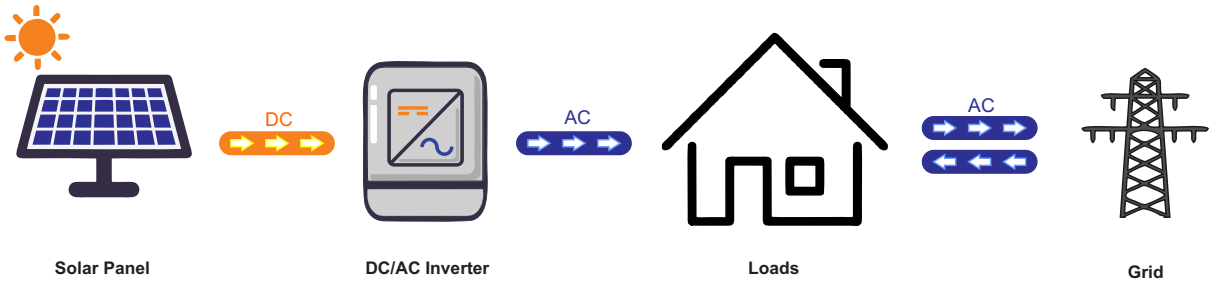

Figure 1.4: Photovoltaic conversion system.

1.2.1 Photovoltaic Modules

The photovoltaic cell, also called the solar cell, is an electronic device that converts sunlight directly into electricity. This technology was invented in 1954 at Bell Telephone Laboratories in the United States [3].

The photovoltaic modules are composed of several photovoltaic cells connected in series and in parallel. The type of connection depends on the voltage and current for which the energy processing system is to operate. The correct choice of the values of these electrical variables is of fundamental importance to determine the efficiency of the converters that condition the energy produced to feed the AC mains, loads, or recharge the battery [8].

The photovoltaic modules behave as a non-linear source and, as you can see in Figure 1.5, depending on the incident radiation and temperature, their electrical characteristics undergo great changes. This characteristic means that they are usually not used directly as an energy source, as the output power depends on several variables, such as the load to which it is

connected and climatic conditions [6]. Due to these characteristics, energy converters are used.

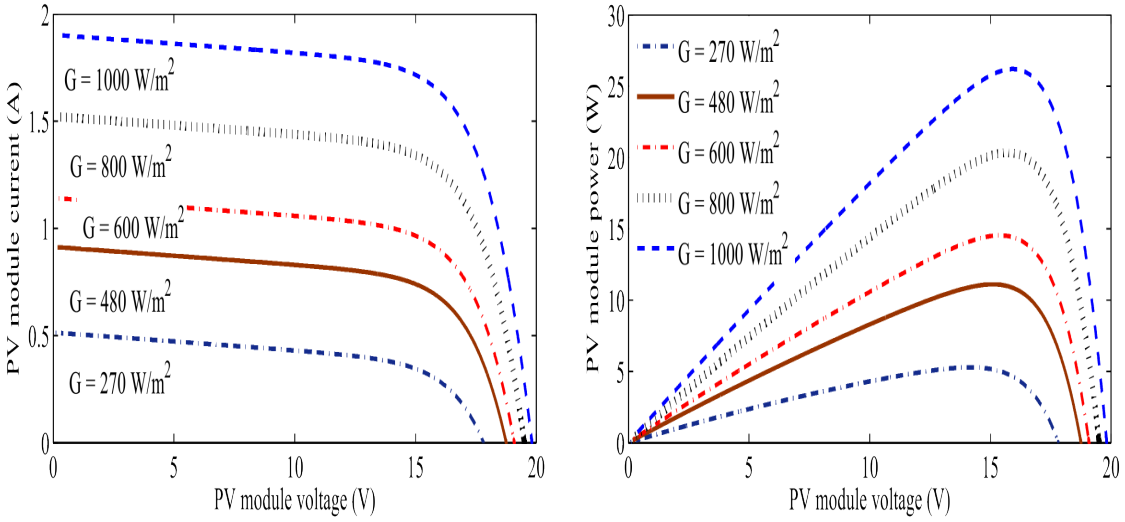

(a) I-V curve (b) P-V curve

Figure 1.5: Characteristics of a PV module for different radiations: (a) I-V curve and (b) P-V curve.

1.2.2 Photovoltaic Inverter

In some cases, a photovoltaic string is connected directly, however most are equipped with energy conditioning circuits between the generation stage and the loads [9]. The photovoltaic inverter is the equipment that conducts this energy conditioning of the system, especially those connected to the grid. Its main function is to convert the DC energy, generated by the PV panels, into AC energy, synchronized with the grid [10]. These devices have a great impact on the photovoltaic system, since the cost of the technology is linked to its efficiency. In addition, the photovoltaic modules are not linear sources, as shown in Figure 1.5, and their electrical characteristics suffer great variation with climatic changes. Inverters have different conversion stages, but normally, they have DC / DC converters operated with MPPT algorithm, to circumvent changes in the characteristics of the source and extract the maximum available power [9].

When the inverter does not have an MPPT algorithm to operate at the maximum power point, the photovoltaic system can have its efficiency drastically reduced, since the mpp changes according to the climatic conditions.

1.2.3 Maximum Power Point Tracking (MPPT)

The output of the photovoltaic cells has limited current, voltage and power. In a stable state of solar irradiance and cell temperature, there is a single point of operation where the voltage and current output results in the maximum output power. When a power cell voltage graph of a photovoltaic cell is plotted, generating the P-V curve, the peak power can be easily recognized.

In most photovoltaic systems, an MPPT algorithm is employed for the maximum available power to be used. The real-time operation is to control the power interface on the PV side so that the operational characteristics of the load and the photovoltaic panel are always combined in the MPP. The purpose of the control is to maximize the production of energy to obtain the highest energy extracted at any time.

1.3 Objectives

The mains objectives of this work are as follows:

- Perform tests with commercial PV inverters, observing their behavior when connected to a PV string and injecting power into the power grid. In this way, to verify the behavior of the MPPT algorithms present in commercial PV inverters available in the laboratory for testing.
- Analysis between four MPPT algorithms, which are widely discussed in the literature: Pertub & Observe, Incremental Condutance, Particle Swarm Optimization and Fuzzy Logic Controller. These techniques are analyzed based on experiments that guarantee similar test conditions for each of the MPPT algorithms, in order to verify the performance of each technique. The tests are defined as follows:
  - Tests with constant conditions of radiation and temperature on the photovoltaic panels: This test makes it possible to compare the oscillation and precision in reaching the maximum power point (MPP);
  - Tests with partial shading conditions: This test verifies which technique is capable of solving the problems generated by shading in part of the PV string and reaching the point of maximum global power (GMPPT).
- Experimental validation and analysis with the control interface, in real time, integrated with Simulink®, and with a POWEREX power kit, which includes a power module with a DC / DC converter and a voltage inverter. The ControlDesk program was also used with the dSPACE controller to develop the monitoring and control interface at the user level.

1.4 Thesis structure

- Chapter 1: Introduction
  - Contains contextualization about the current panorama of photovoltaic energy in energy matrix and the role of maximum power algorithms in a system photovoltaic.
- Chapter 2: State of art
  - Contains review of the literature on MPPT algorithms for inverters connected to the grid, mainly the four techniques used for the analysis: Pertub & Observe, Incremental Condutance, Particle Swarm Optimization and Fuzzy Logic Controller.
- Chapter 3: Theoretical background
  - It contains a brief explanation of theoretical concepts that helped in the construction of the thesis, such as Modeling a cell, Boost Converter and Proportional Integral Derivative Control.
- Chapter 4: Methodology
  - It shows the power structure used, its relevant components and the implementation of MPPT algorithms.
- Chapter 5: Experimental results
  - Contains the results obtained from the implementation of MPPT algorithms with dSPACE, a real-time control interface, and with the proposed power structure.
- Chapter 6: Analysis and discussion
- Chapter 7: Conclusion

Chapter 2

State of the Art

This chapter presents the state of the art of algorithms for tracking the maximum power point applied to photovoltaic inverters, explaining the different techniques commonly used.

2.1 MPPT algorithms

The first MPPT system was introduced in 1968 for a space system, over the years, several MPPT algorithms have been developed and widely adapted to determine the maximum power point, mainly for applications in photovoltaic inverters. The most used control techniques consist of acting automatically in the duty cycle, reaching the ideal point of the source, regardless of variations in weather conditions or sudden changes in loads, which can occur at any time [11].

This control for tracking the maximum power point places the system operating as close as possible to the voltage and the current at the maximum power point (MPP), respectively, V_{mpp} and I_{mpp}. The principle used in the MPPT technique is to match the conductance or resistance between the source and the load. In systems connected to the grid, the relationship between the load and the generator is not direct, so in this case, the load is equivalent to the power extracted from the photovoltaic generation [11].

Most loads powered by a PV source require variable voltage or current. When they are directly coupled to the photovoltaic generator, their impedance cannot always be adjusted for the purposes of the MPPT. However, when a power interface is connected between the load and photovoltaic generator, load conductance or impedance in the photovoltaic generator can vary through energy conversion. Evolution is demonstrated in Figure 2.1, in which a power interface is used between the photovoltaic generator and the load.

With a fixed load, as illustrated in Figure 1.5 (a), the characteristics VI are defined by the

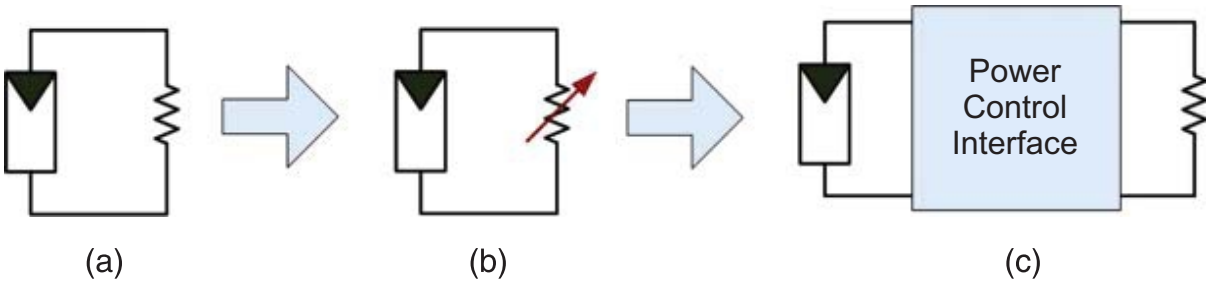

Figure 2.1: Evolution of maximum power point tracking: (a) Fixed load; b) Variable load; (c) Controllable power interface.

source and it is not possible to track the maximum power, in Figure 1.5 (b), the operating point can be changed by varying the load resistance, but it is necessary to find the MPP point manually, since it is not fixed and changes according to the weather conditions to which the PV cells are exposed.

A power converter, as shown in Figure 1.5 (b), can change the I-V characteristics of the input to the output and provide equivalent resistance to match the MPP point on the PV output terminal. This is the fundamental approach in the latest MPPT technologies [9].

The solar irradiance and the cell temperature significantly affect the MPP. Dynamic tracking is necessary to track unpredictable changes in environmental conditions, particularly solar irradiance, as the cell temperature generally varies with a slower dynamic than irradiance. Furthermore, the diversity of materials used in the construction of a photovoltaic cell means that each one has different V-I characteristics[9]. Switched power converters are generally used as an interface for the generation of photovoltaic energy. Using these electronic circuits, unwanted ripples can appear at the output terminals of the photovoltaic modules, thus making dynamic tracking difficult and reducing their efficiency.

The main components of the MPPT circuit are its power stage and the controller. The configuration of the MPPT scheme is represented in Figure 2.2. The input voltage of the power stage V_{pv} and the current I_{pv} are used by the controller for MPP tracking purposes. In this case, the control of the power stage, based on the voltage or current, where they are changed continuously until the photovoltaic panel reaches or is close to its MPP [11].

Many methods have been developed to determine the maximum power point, some of which are:

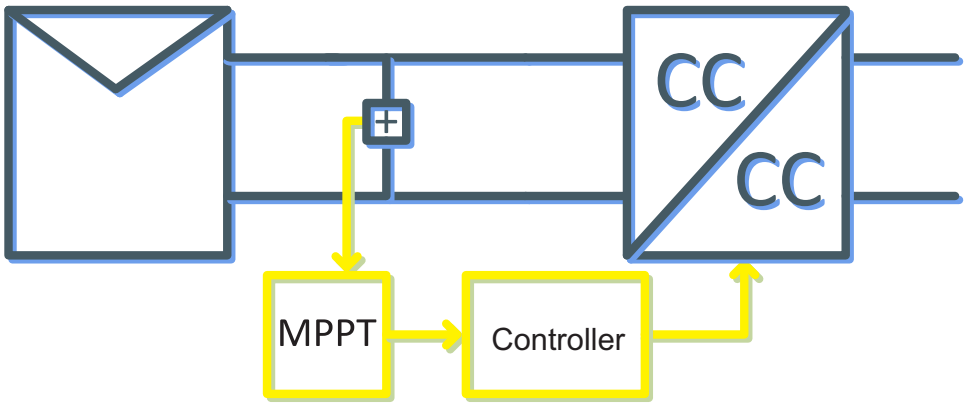

Figure 2.2: System with power interface and MPPT.

- MPPT control based on proportionality relationships.
- Perturb & Observe.
- Incremental Conductance.
- MPPT control based on Optimization algorithms.
  - *Particle swarm optimization (PSO).*
- MPPT control based on artificial neural networks.
- Fuzzy Logic Controller.

2.2 MPPT Based on Proportionality Relationships

These methods are based on the electrical characteristics of the photovoltaic modules, V_{oc} and I_{sc} and, based on these values, define an operating point. These algorithms that work in open loop and have low execution complexity.

For the implementation of this technique, it is considered that the temperature is constant or as it varies slowly, and that the radiation changes are not large enough to alter the characteristics of the MPP.

The Figure 2.3 shows the variation of MPP as a function of radiation and temperature.

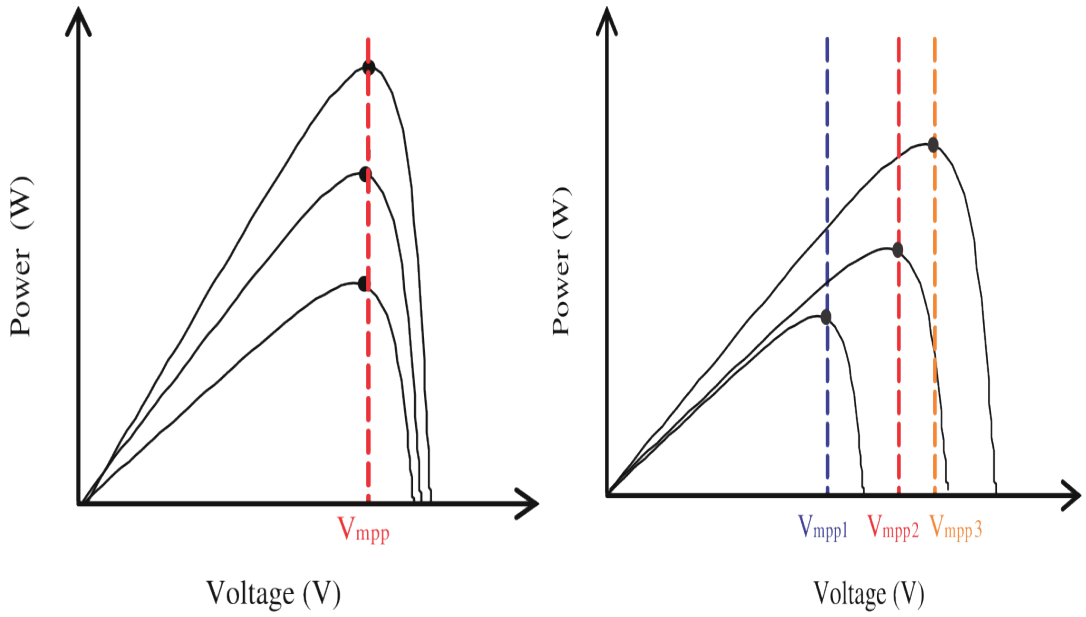

(a) Variable radiation and fixed temperature (b) Fixed radiation and variable temperature

Figure 2.3: Characteristics of the PV curve with: (a) Variable radiation and fixed temperature; (b) Fixed radiation and variable temperature [11].

2.2.1 Constant Reference Voltage Algorithm

It is one of the simplest techniques, which consists of comparing the voltage of the panel V_{pv} with a reference voltage corresponding to an ideal voltage V_{mpp}. The error between these voltage values is used to adjust the operation of the power converter. The reference voltage is given by the following equation:

$$V_{\text{ref}} = K_1 . V_{\text{oc}} \tag{2.1}$$

where K_1 is a constant ($0.71<K_1<0.78$) [11].

2.2.2 Constant Reference Current Algorithm

It is also one of the simplest techniques, similar to the method discussed in 2.2.1, which consists of comparing the output current of the panel I_{pv} with a reference voltage corresponding to an ideal current I_{mpp}. The error between these current values is used to adjust the operation of the power converter. The reference current is given by the following equation:

$$I_{\text{ref}} = K_2 . I_{\text{sc}} \tag{2.2}$$

where K_2 is a constant ($0.78<K_2<0.92$) [11].

2.3 Perturb & Observe

The Perturb & Observe (P&O) method is the most popular algorithm and belongs to the class of direct MPPT techniques. This technique applies a small disturbance to the system in order to follow the path that leads to the point of maximum power [11].

It is a widely used algorithm due to its ease of implementation. This is a continuous process of observation and disturbance until the point of operation converges to the MPP [12].

As it can be seen from the flowchart of Figure 2.4, the algorithm compares the power and voltage at time *k* with the samples at time *k-1* and, based on this information, it traces the path for MPP. A small voltage disturbance alters the power of the photovoltaic panel. If this power change is positive, the algorithm continues to increase the voltage, but if the power change is negative, this indicates that the MPP is in the opposite direction, so the algorithm starts to decrease the voltage. In this way, part of the PV curve is checked for small disturbances to find the point of maximum power.

The greater these disturbances, the faster the MPP is reached, however, the greater the oscillation around it.

Many researches propose modifications to the P&O algorithm to overcome problems such as oscillations around the MPP and its response time during variations in the power curve [12].

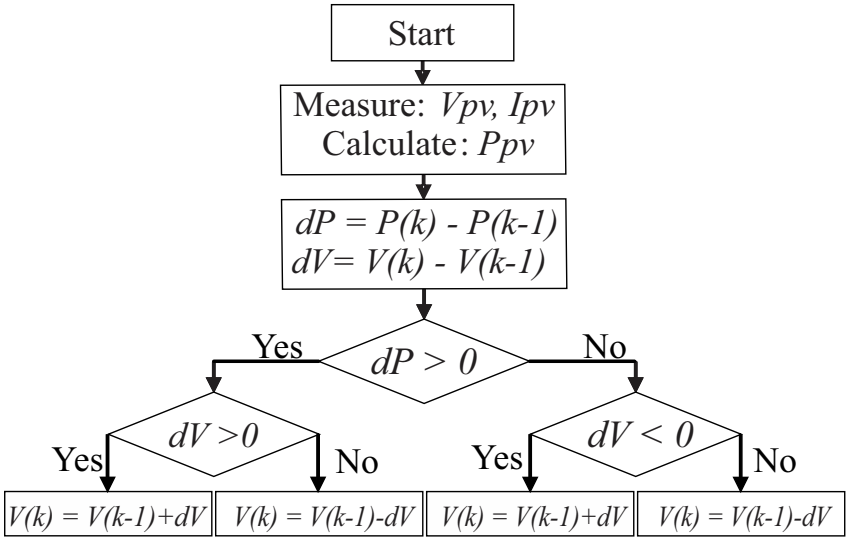

Figure 2.4: Flowchart of MPPT P&O.

In this case, the control is done by voltage, and for the current control case, the reasoning analogous to that shown in the flowchart of Figure 2.4 is used. However the P-I curve is almost constant to the left of the MPP, which makes the use of the current reference unviable.

2.4 Incremental Conductance

The Incremental Conductance method is a technique that requires greater precision from the sensors and focuses directly on variations in power [7]. This algorithm requires voltage and current readings from the output of the photovoltaic modules to calculate the conductance, equation 2.3, and the incremental conductance, equation 2.4.

By comparing the values obtained, the decision is made to increase or decrease the PV voltage to track the MPP.

$$GG = I_{\text{pv}} / V_{\text{pv}} \tag{2.3}$$

$$\Delta GG = \Delta I_{\text{pv}} / \Delta V_{\text{pv}} \tag{2.4}$$

The decision to increase or decrease the voltage is made based on the characteristic derivatives, P-V or P-I of the PV string. Through the curve, it is observed that, when the operating point is to the left of the MPP, the value of the derivative of the curve, in relation to the voltage or current, assumes a negative value, while the point is to the right of the MPP, the derivative assumes positive value, and when working in MPP, it assumes zero value, as shown in the equation 2.5.

$$\begin{cases} \Delta GG = -GG, & \text{in MPP} \\ \Delta GG > -GG, & \text{left of the MPP} \\ \Delta GG < -GG, & \text{right of the MPP} \end{cases} \tag{2.5}$$

The algorithms work as shown in the flowchart of Figure 2.5, comparing the conductance and the incremental conductance to decide when to increase or decrease the PV voltage to track the MPP [11].

In this case, the control is done under voltage, and for the current control case, the reasoning analogous to that shown in the flowchart of Figure 2.5 is used. However the P-I curve is almost constant to the left of the MPP, which makes the use of the current reference unviable.

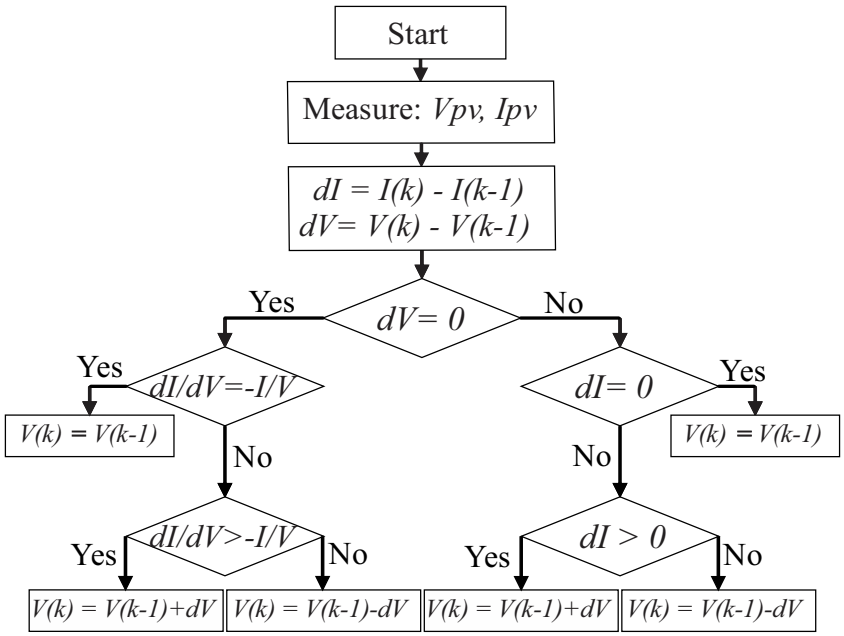

Figure 2.5: Flowchart of MPPT IC.

2.5 Particle Swarm Optimization

Particle Swarm Optimization (PSO) is one of the swarm intelligence techniques that uses stochastic variables based on population for solving optimization problems [7].

This algorithm was developed by Kennedy and Eberhart in 1995 and works by researching the space of a function, adjusting the trajectories of individual agents, called particles, because these trajectories form fragmented paths in an almost stochastic manner. Each particle is attracted to the position of the maximum global, and the best location in history, and at the same time, it has a tendency to move randomly [13].

The PSO algorithm was not designed for applications in photovoltaic systems, however it can be adapted to work as an MPPT algorithm. This technique works by searching the space of a function, using particles and each one has its position adjusted as better points are found. In PV application, it correspond to adjust the duty cycle of the DC-DC converter for each particle at a point on the PV curve, looking for the point of maximum power.

The population is called the swarm and its individuals are called the particles [13]. The swarm is defined as a set in equation 2.6, N is the number of particles, and each one is

associated with a duty cycle, which assume equidistant values during initialization, values between 0 to 1, respecting the limitations of the DC converter used.

$$D = \{d_1, d_2, ..., d_{\mathrm{i}}\}, \qquad i = 1, 2, ... N \tag{2.6}$$

When imposing a duty cycle, the algorithm makes that, analogously, we have a function of the power extracted by the duty cycle, as shown in the equation 2.7.

$$f(D(\mathrm{i})) = p_{\mathrm{i}}, \qquad i = 1, 2, ... N \tag{2.7}$$

The algorithm works with iterations, and during each one, the dutty cycle of each particle is used, so that afterwards it is compared to was the one that obtained the best result, in this case, the best power [14]. The duty cycle that provides the best value during each iteration is stored in the variable G_{b}, equation 2.8, and the best value for each particle is stored in the vector p_{bi}, as shown in the equation 2.9.

$$G_{\mathrm{b}} = max(f(D(\mathrm{i}))) \tag{2.8}$$

$$p_{\mathrm{bi}} = [max(p_1),\ max(p_2),\ ...\ max(p_{\mathrm{N}})], \qquad i = 1, 2, ... N \tag{2.9}$$

It is assumed that the particles move within the P-V curve, iteratively. This is possible by adjusting its position. This adjustment is called speed, described by the equation 2.10, where R_1 and R_2 are random values between 0 and 1. The parameters c_1 and c_2, are the acceleration constants or learning parameters. They typically use $c_1 \approx c_2 \approx 2$ [13]. During the first iteration, the speed assigned to each particle is 0.

$$v_{\mathrm{i}}(t+1) = v_{\mathrm{i}}(t) + c_1 R_1\ (p_{\mathrm{bi}}(t) - d_{\mathrm{i}}(t)) + c_2 R_2\ (G_{\mathrm{b}}(t) - d_{\mathrm{i}}(t)) \tag{2.10}$$

Each particle has a speed adjustment according to its duty cycle and previous position. The adjustment is given by the equation 2.11.

$$d_{\mathrm{i}}(t+1) = d_{\mathrm{i}}(t) + v_{\mathrm{i}}(t+1) \tag{2.11}$$

The flowchart shown in Figure 2.6, illustrates the process of each iteration of the PSO algorithm.

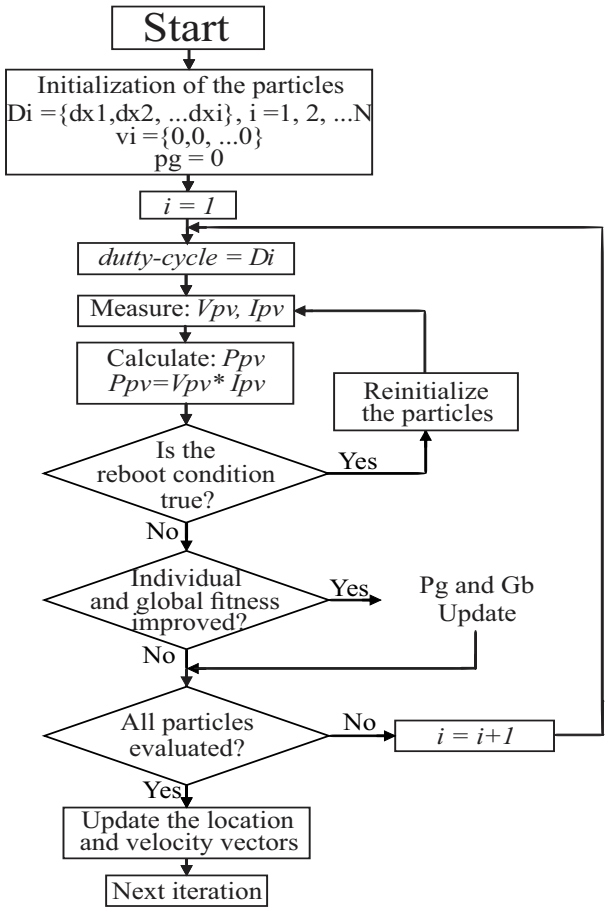

Figure 2.6: Fluxograma do MPPT PSO.

2.6 Fuzzy Logic Controller

Fuzzy logic is a part of artificial intelligence associated with reasoning algorithms and its main objective is to imitate human thought patterns and their decision-making skills [15]. Fuzzy logic algorithms are often used in situations where process data in binary form are not applicable for finding a solution. the FLC can translate inaccurate statements into concepts that are more accurate, and therefore, make logical sense. So, for example, when we discuss distance, a nearby location, for a controller with fuzzy logic, has an indication of the degree of distance between near and far. Knowing this information, the distance is more precisely determined, and, in terms of binary logic, we would have only two answers, which are near or far.

The Fuzzy logic controller algorithm (FLC) is divided into 3 main parts, which are: fuzzification, rule base and defuzzification. Figure 2.7 shows the block diagram of the algorithm.

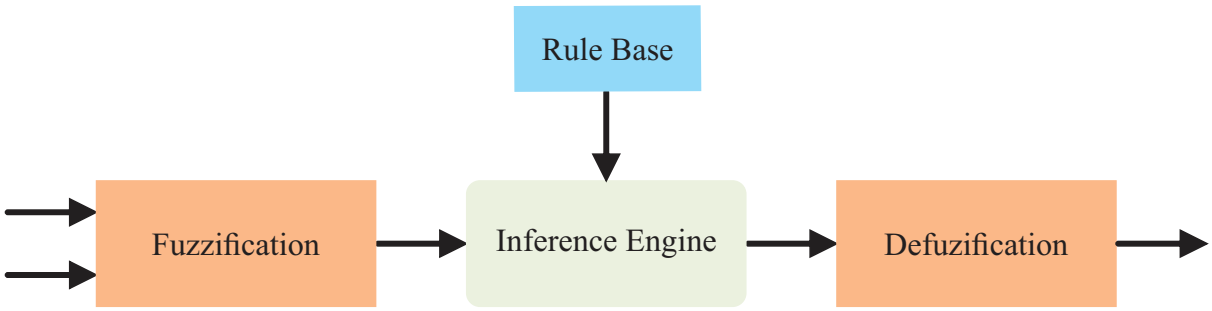

Figure 2.7: Flowchart of MPPT FLC.

For applications in MPPT algorithms with FLC, two numerical inputs are generally used: the voltage variation, ΔV_{pv}, and power variation, ΔP_{pv}, as show by equations 2.13 and 2.12.

$$\Delta V_{\text{pv}} = \Delta V_{\text{pv}}(t) - \Delta V_{\text{pv}}(t-1) \tag{2.12}$$

$$\Delta P_{\text{pv}} = \Delta P_{\text{pv}}(t) - \Delta P_{\text{pv}}(t-1) \tag{2.13}$$

During the first stage, fuzification, the numeric entries are converted into linguistic variables based on membership functions [15].

In this stage, triangular association functions can be used for the inputs and also for the

outputs. The two input variables are converted into linguistic values: Large Negative (NB), Small Negative (NS), Zero (ZE), Small Positive (PS) and Large Positive (PB) [16]. Mamdani's method is commonly used for fuzzy inference. The Defuzzification, the centroid method. The rule base is given based on the application.

Chapter 3

Modeling a PV panel and Power Interfaces

This chapter presents concepts relevant to understanding how photovoltaic modules and power interfaces can be modeled and controlled.

3.1 Modeling a PV module

The PV solar module can be represented as an ideal PV solar cell with a current source I_{ph}, parallel to a diode as shown in Figure 3.1 [17].

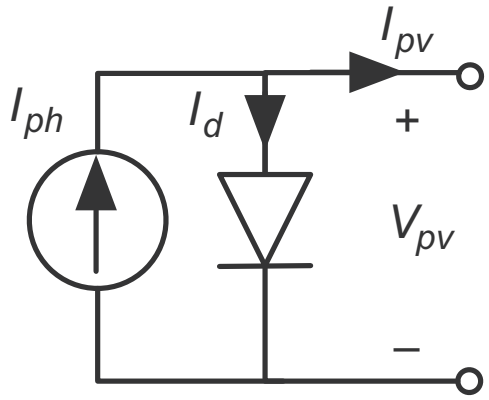

Figure 3.1: Equivalent circuit of ideal model.

Using Kirchhoff's first law, the output current can be described:

$$I_{\mathrm{pv}} = I_{\mathrm{ph}} - I_{\mathrm{d}} \tag{3.1}$$

From semiconductor theory, the fundamental mathematical equation that describes the I–V characteristic of the photovoltaic, known as the Shockley diode current, is shown by the equation 3.2 [18].

$$I_{\mathrm{d}} = I_{\mathrm{s}} * \left[\exp\left(\frac{qV_{\mathrm{oc}}}{N_{\mathrm{s}} K A T_0} \right) - 1 \right] \tag{3.2}$$

Using the equation 3.1 in 3.2, equation is obtained:

$$I_{\mathrm{ph}} = I_{\mathrm{ph}} - I_{\mathrm{s}} * \left[\exp\left(\frac{qV_{\mathrm{oc}}}{N_{\mathrm{s}} K A T_0} \right) - 1 \right] \tag{3.3}$$

For any physical system, PV cells can be modeled with different levels of accuracy [19]. In the ideal case, the solar cell provides a very good approximation current generated by photons, which is directly proportional to lighting intensity and irradiance [17]. This model does not take into account parameters present in the behavior of a real PV cell. For this, there are more realistic models, such as the single diode model (SDM), with shunt and series resistances, that is generally used to model monocrystalline silicon cells [19]. The equivalent circuit of this model is shown in Figure 3.2, in which the addition of a series resistance R_s and parallel resistance R_p to the ideal model, already shown in Figure 3.1.

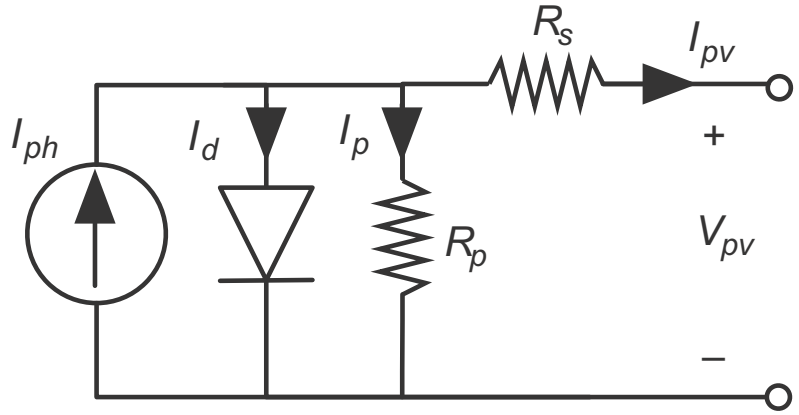

Figure 3.2: Equivalent circuit of single-diode model.

The series resistance R_s represents the voltage drop in in semiconductors, metallic parts and circuit connections. R_p is the parallel resistance and is associated with the infiltration current due to the cell thickness, and assumes high resistance values.

Considering R_s, and how R_p assuming high values, the model can be simplified considering as an infinite resistance value. Current equation of the diode 3.2 is now given by the equation 3.4.

$$I_{\mathrm{d}} = I_{\mathrm{s}} * \left[\exp\left(\frac{q V_{\mathrm{oc}} + I_{\mathrm{pv}} R_{\mathrm{s}}}{N_{\mathrm{s}} k A T_0} \right) - 1 \right] \tag{3.4}$$

With this change, the current I_{pv} is given by the equation 3.5.

$$I_{\mathrm{pv}} = I_{\mathrm{ph}} - I_{\mathrm{s}} * \left[\exp\left(\frac{q V_{\mathrm{oc}} + I_{\mathrm{pv}} R_{\mathrm{s}}}{N_{\mathrm{s}} k A T_0} \right) - 1 \right] \tag{3.5}$$

In modeling PV cells, there are parameters that need to be determined. These parameters depend on the selected model of the PV module. The photocurrent, I_{ph}, is linearly dependent on solar radiation and influenced by temperature, as described by the equation 3.6.

$$I_{\mathrm{pv}} = I_{\mathrm{sc}} + k(T_0 - T_{\mathrm{r}}) * \left(\frac{G}{G_{\mathrm{ref}}} \right) \tag{3.6}$$

The reverse saturation current I_{rs} and the saturation current I_s are calculated using:

$$I_{\mathrm{rs}} = I_{\mathrm{sc}} / \left[\exp\left(\frac{q V_{\mathrm{oc}}}{N_{\mathrm{s}} k A T_0} \right) - 1 \right] \tag{3.7}$$

$$I_{\mathrm{s}} = I_{\mathrm{rs}} * \left[\frac{T_0}{T_{\mathrm{r}}} \right]^3 * \exp\left[\left(\frac{q E \mathrm{g}}{A k} - \frac{1}{T_0} \right) \left(\frac{1}{T_{\mathrm{r}}} - \frac{1}{T_0} \right) \right] \tag{3.8}$$

Where A is the ideality factor of the diode and Eg the energy band gap. All of these values refer to the chosen module model and its manufacturing characteristics.

I_{ph}: Current generated by the incident light[A]

I_d: Diode saturation current[A]

R_s: Cell parallel(shunt) resistance[ohm]

R_h: Cell series resistance[ohm]

N_s: Number of PV Cells connected in series

A: Diode quality(ideality) factor

k: Boltzmann's constant(1.381×10e-23) [J/K]

q: Charge of the electron(1.602×10e-19) [C]

T_0: Kelvin Temperature at standard test condition [K]

3.2 Boost Converter

The Boost converter is used to raise the input voltage to the desired voltage. The input for this converter can be from any DC source like solar modules. The circuit diagram of the Boost converter is shown in Figure 3.3.

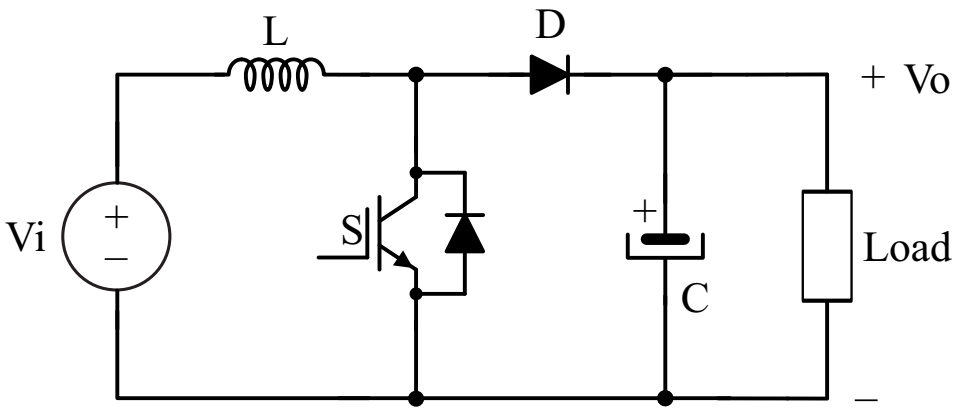

Figure 3.3: Circuit of Boost converter.

With switch S closed, the inductor is charged by the input source and stores energy. In this mode, the energy stored in the inductor gradually increases, so the charge and discharge of the inductor can be considered linear. The diode, on the other hand, blocks the flow of current, and thus the load current supplied remains almost constant due to capacitor discharge [20].

When switch S is open, the diode becomes polarized. The energy stored in the inductor is discharged through the diode and charges the capacitor. The capacitor now supplies voltage when charged. The charging current remains almost constant throughout the operation [20].

Equating the output and input voltage of the Boost converter, and D being the duty cycle of switch S, we have:

$$V_0 = \left(\frac{V_i}{1-D}\right) \tag{3.9}$$

In general, PV string inverters have a boost converter at the input. It is responsible for adjusting the duty cycle in order to fix the point of operation of the row, very close to the point of maximum power. This setting of the operating point is what is called the MPPT algorithm.

3.3 Proportional Integral Derivative Control (PID)

A PID controller can be considered an extreme way of a phase compensator with a pole at the origin and the other in infinity. Likewise, the PI controller, and the PD can also be considered as extreme form of delay compensator or phase advance, respectively. Figure 3.4 shows the block diagram of a parallel PID controller [21].

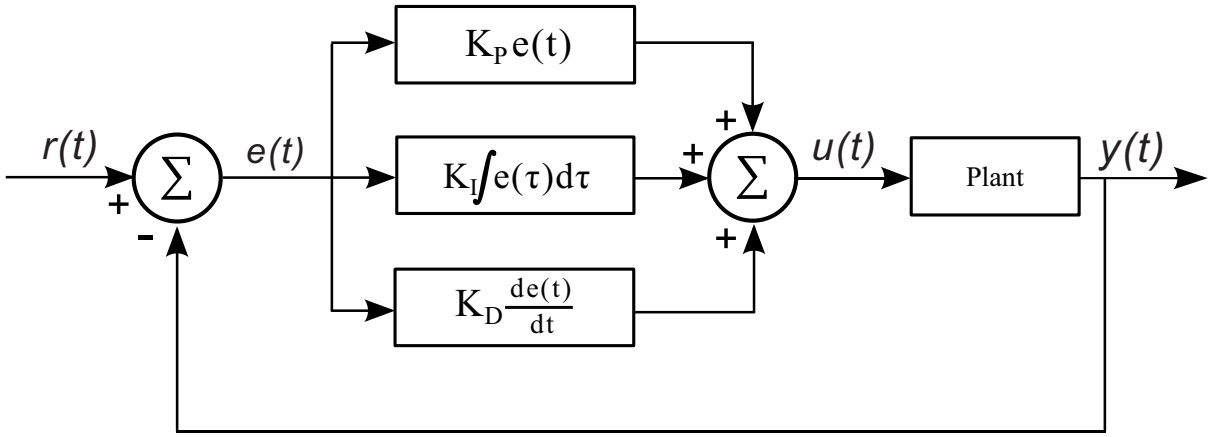

Figure 3.4: Parallel PID Controller.

A standard PID controller has its transfer function usually written in parallel, given by the equation 3.10. Using the proportional, integral and derivative gains.

$$G(s) = K_P + K_I \left[\frac{1}{s}\right] + K_D s \tag{3.10}$$

The three gains are highlighted by the following:

• Proportional gain (K_P) - action proportional to the error signal through the gain factor.

• Integral gain (K_I) - reduces steady-state error through a low frequency compensation by an integrator.

• Derivative gain (K_D) - improves transient response through high frequency compensation by a differentiator.

The PI controller, which is derived from the PID, can be used to control power converters. The Figure 3.5 shows an example of application of the control, where a PI controls the input voltage of the DC / DC converter based on the voltage reference decided by an MPPT

algorithm.

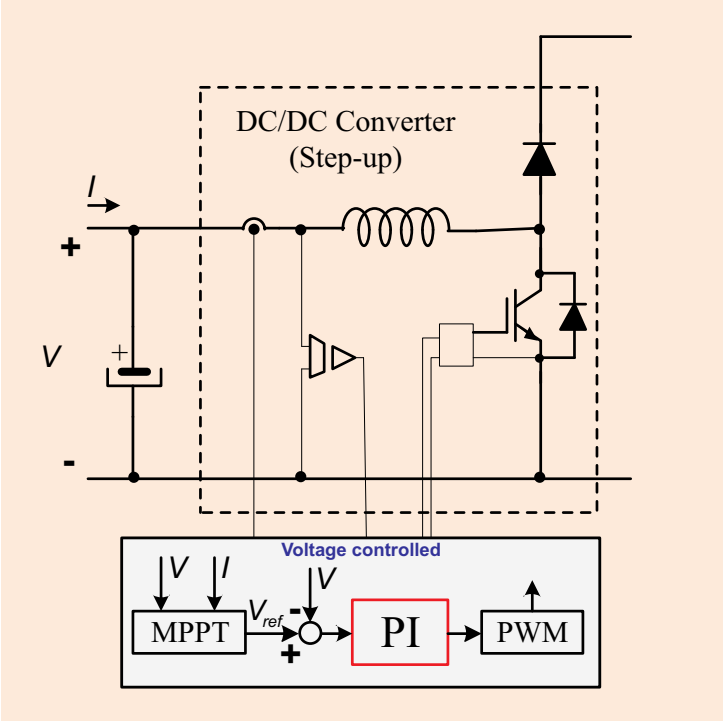

Figure 3.5: Parallel PID Controller.

Chapter 4

Experimental tests of MPPT algorithms

This chapter describes the power converter topology used during the tests and its relevant components, such as the DC-DC and DC-AC converters and their control algorithms, photovoltaic modules and power grid. Commercial PV inverters used in the tests and their characteristics are also described.

4.1 Power converter topology

The converter topology used for the experimental tests of the MPPT algorithms, follows the simplified block diagram, shown in Figure 4.1, composed of a photovoltaic string, followed by a bidirectional DC-DC converter, configured as a converter Boost, then a full bridge DC-AC inverter and an LC filter, before connection to the grid.

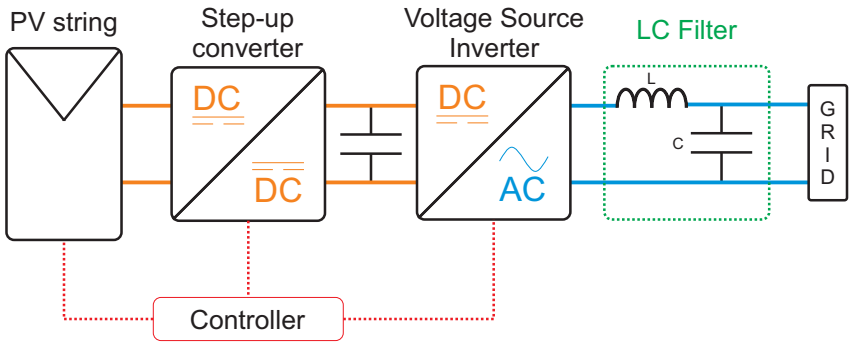

Figure 4.1: Block diagram of the power structure.

The structure with all the electrical connections and topologies of the converters is shown in Figure 4.2. In the next topics, additional explanations about the most relevant parts of the applied power topology and the components used in the tests are presented.

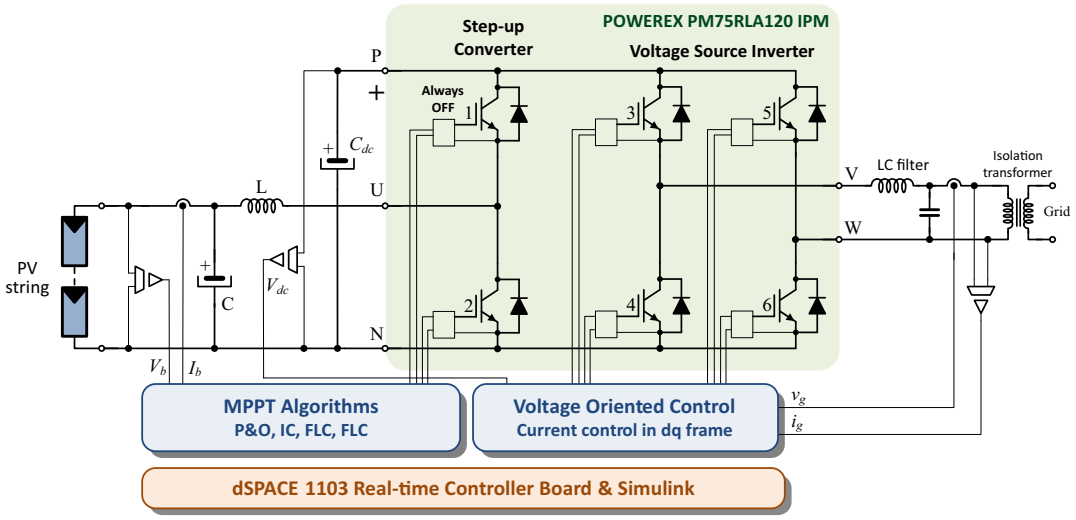

Figure 4.2: Power converter topology.

4.1.1 Photovoltaic Strings

For the tests, two PV strings were used, shown in Figure 4.3, which are formed by photovoltaic modules of different number and models. The String A model is composed of 5 Fluitecnik FTS220P modules, while String B is composed of 3 REC Solar REC275PE modules.

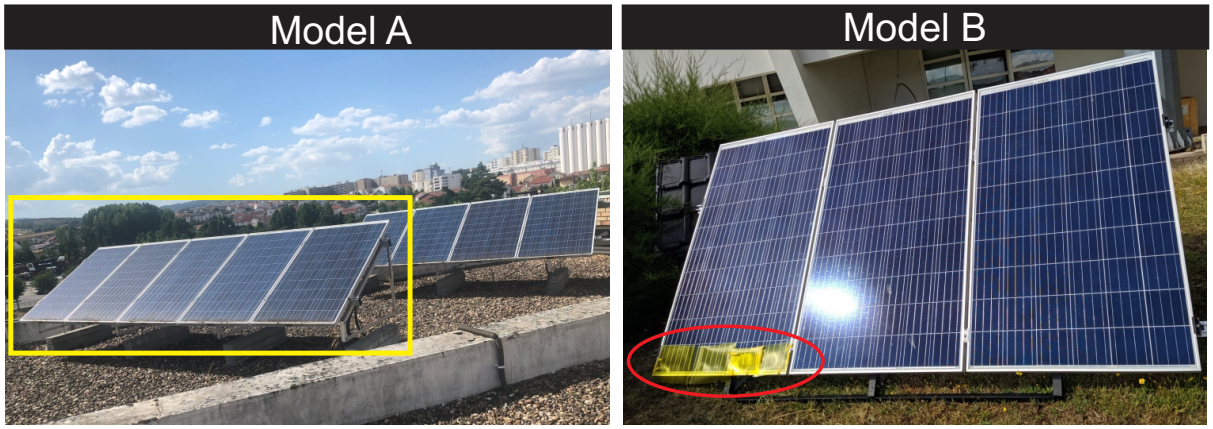

Figure 4.3: String A (on the left) and string B (on the right).

Model B was used only for tests, in which part of the string must be partially shaded. In Figure 4.3 it is possible to observe the shaded part, highlighted by a red circle. As one of the 3 panels of the string model B is shaded and the PV curve has two peaks. This is because when a cell is shaded, that is, less radiation hits its surface, and even though it operates at a voltage

lower than the open circuit voltage, V_{oc}, the current reaches zero, and the cell stops driving. The lower the radiation, the lower the voltage value for the cell to stop conducting.

Table 4.1: Characteristics of Photovotaic Models.

PV modules of	Max. Power	I_{SC}	V_{OC}	I_{MPP}	V_{MPP}
String A	220 W	8.30 A	36.76 V	7.51 A	29.38 V
String B	275 W	9.25 A	38.70 V	8.74 A	31.50 V

4.1.2 DC-DC converter

The DC-DC power converter used follows the topology of the Boost converter, responsible for imposing a voltage on the photovoltaic string. This voltage at the converter input is controlled by the MPPT algorithm.

In the power structure, one of the three legs of a three-phase photovoltaic inverter is used, as shown in Figure 4.2, using the IGBT switch S_1 always off and controlling by PWM the IGBT S_2 key. The converter uses a $12mH$ inductor (L) and a 1000 μF output capacitor C_{dc}, which stores the energy and separates the DC-DC conversion stage from DC-AC.

4.1.3 DC-AC converter

The DC-AC power converter, is a single-phase full bridge voltage source inverter, is a bridge inverter complete with IGBTs, used for the injection of the active power extracted from the photovoltaic matrix in to the grind, with the possibility of controlling the reactive power. For this converter two arms of the three-phase inverter are used, which correspond to the keys S_3, S_4, S_5 and S_6, which are controlled based on Voltage Oriented Control.

4.1.4 Grid connection

The grid can be represented by an AC source, with the ability to exchange any amount of active and reactive power. In practical terms, the micro grid installed in the IPB LSE laboratory, for educational and research purposes.

4.2 Testing platform

The test platform used follows the inverting topology and control strategy shown in Figure 4.2, which is implemented as shown in Figure 4.4.

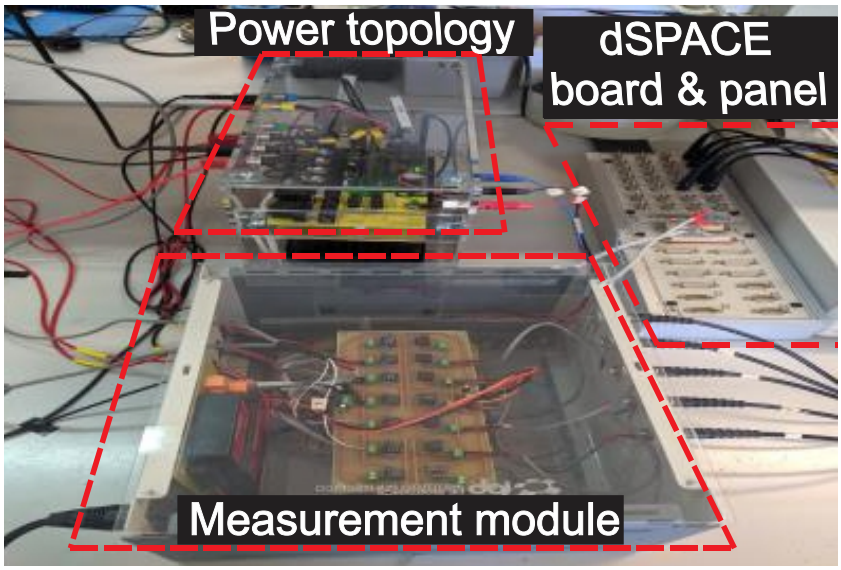

Figure 4.4: Testing platform.

The power converter is based on the Powerex PM75RL1A20 intelligent power module shown in Figure 4.5, with a 3-phase IGBT voltage source inverter with the BP7B isolation circuit shown in Figure 4.6. A leg is used for the boost converter, where one of the IGBT's always remains off, functioning as a diode, while the other semiconductor is activated by the MPPT control. The remaining two arms are used as a single-phase full bridge inverter, which is controlled by Voltage Oriented Control.

Figure 4.5: Powerex PM75RL1A20 intelligent power module.

Figure 4.6: BP7B isolation circuit.

The MPPT algorithms and the voltage oriented control were implemented in Simulink®. Then, dSPACE 1103 realtime controller board and ControlDesk® application were used for the real-time control.

The Figure 4.5 shows the test platform, where it is possible to observe the meassurement module, which is necessary to adapt the signals to the reading range of the dSPACE 1103 controller and the entire power circuit, which is based on the Powerex PM75RL1A20 intelligent power module with the BP7B isolation circuit.

4.3 Control Algorithms and implementation

The control techniques used were implemented using the dSPACE 1103 controller board, which is programmed with the Matlab Simulink® software, using the block diagram logic, through the available library. In the implementation, the control of the power topology is divided in two parts, control of the Boost DC-DC converter, by the MPPT algorithm, and control of the DC-AC converter, by the Voltage Oriented Control.

The Figure 4.7 shows the block diagram of the control strategies used.

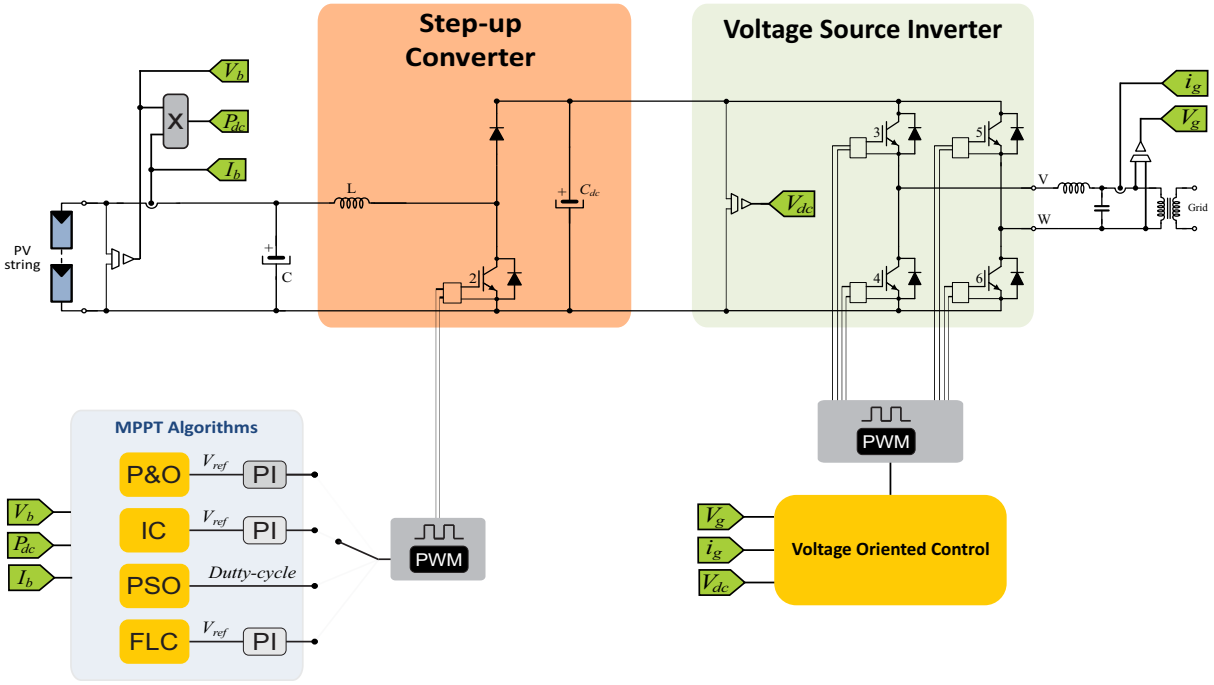

Figure 4.7: Power topology control.

The control of the photovoltaic DC-AC inverter connected to the grid is based on Voltage Oriented Control (VOC). This control strategy uses the transformation of coordinates between two stationary axes $\alpha\beta$ and the synchronous rotating frame dq of reference, where the current is decoupled and controlled separately.

Figure 4.8 shows the Voltage Oriented Control block diagram, similar to that implemented in Simulink®, since the programming logic is also based on the block diagram.

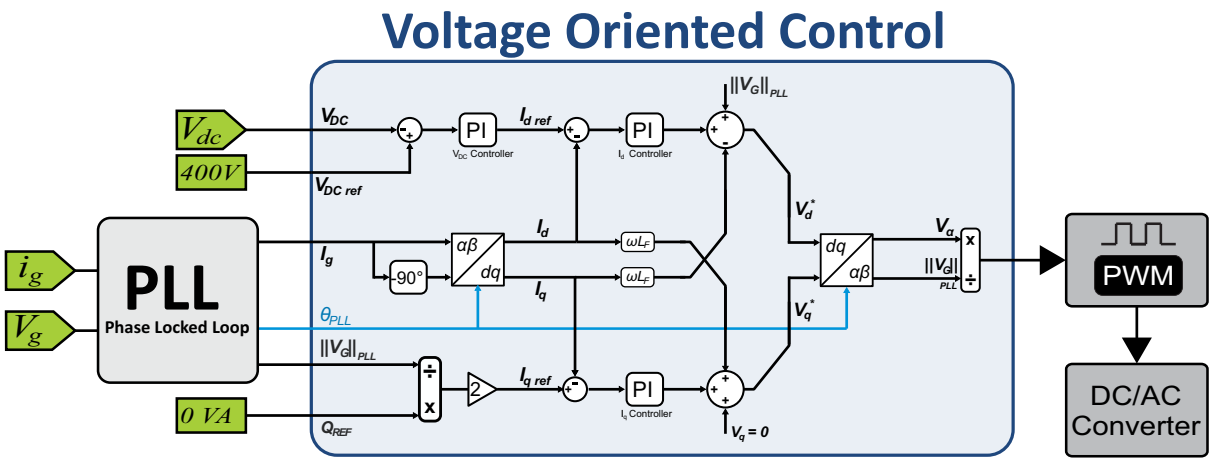

Figure 4.8: Implemented block diagram of Voltage Oriented Control.

The gain values used in PI controllers in Voltage Oriented Control are shown in the Table 4.2.

Table 4.2: Gains from PI controller implemented in Voltage Oriented Control.

PI controller - dq Currents	
Parameter	Experimental Value
kp	20
ki	2000
PI controller - DC link voltage	
Parameter	Experimental Value
kp	0,19
ki	10

The control of the DC-DC converter is performed by one of the four MPPT algorithms used: P&O, IC, PSO and FLC. The Pertub & Observe algorithm is implemented as shown in the block diagram of Figure 4.9, where the algorithm uses the voltage signals V_b and P_{dc} generating a reference in voltage. It is necessary to use a PI controller to control the voltage.

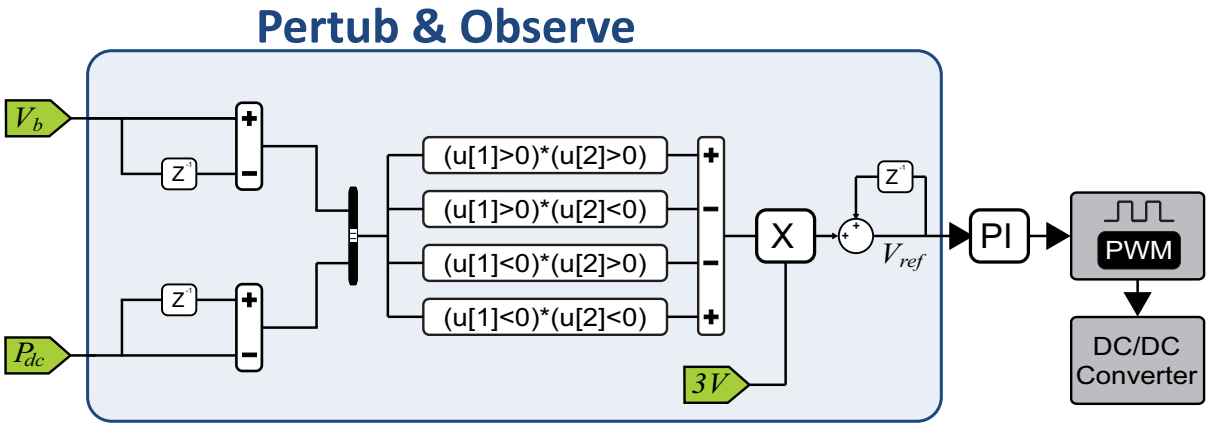

Figure 4.9: Implemented block diagram of P&O.

The gain values used in the PI controller, in the algorithm Pertub & Observe, are shown in Table 4.3.

Table 4.3: Gains from PI controller implemented in the PO algorithm.

PI controller - P&O	
Parameter	Experimental Value
kp	20
ki	2000

The Incremental Conductance algorithm is implemented as shown in Figure 4.10, and also uses two signals, PV array voltage V_b and the power extracted P_{dc}. This technique generates a voltage reference, so it is necessary to use a PI controller to control the voltage.

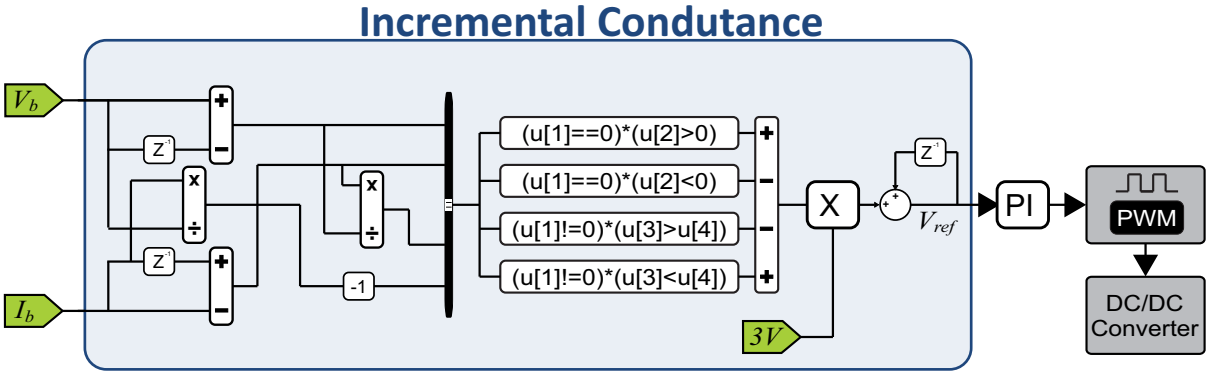

Figure 4.10: Implemented block diagram of IC algorithm.

The gain values used in the PI controller, in the Incremental Condutance algorithm are shown in Table 4.4.

Table 4.4: Gains from PI controller implemented in the IC algorithm.

PI controller - IC	
Parameter	Experimental Value
kp	20
ki	2000 W

The Particle Swarm Optimization algorithm is implemented as shown in Figure 4.14, and also uses the extracted power P_{dc}. This technique does not require the PI controller, as it directly generates the duty cycle reference.

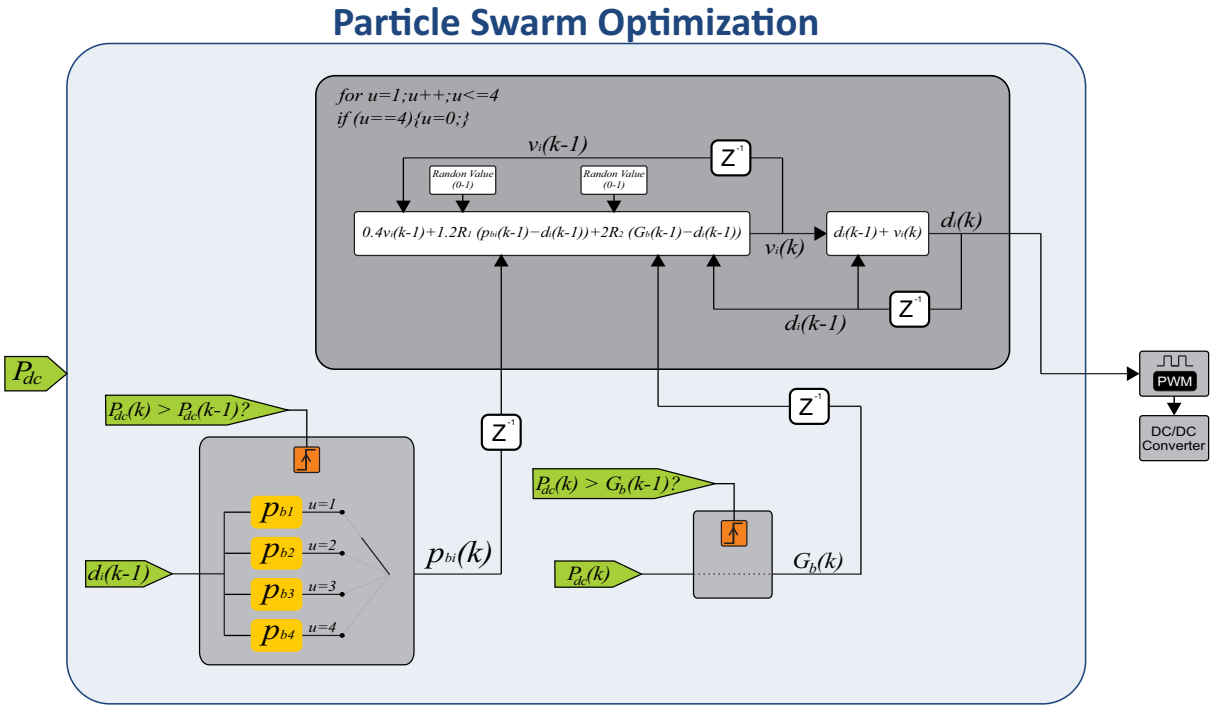

Figure 4.11: Implemented block diagram of PSO.

For the Fuzzy Logic Controller algorithm, triangular association functions shown in Figure 4.12 were used, for inputs and outputs, with the centroid defuzzification method. The basic rule used, empirically obtained, follows that shown in Figure 4.13.

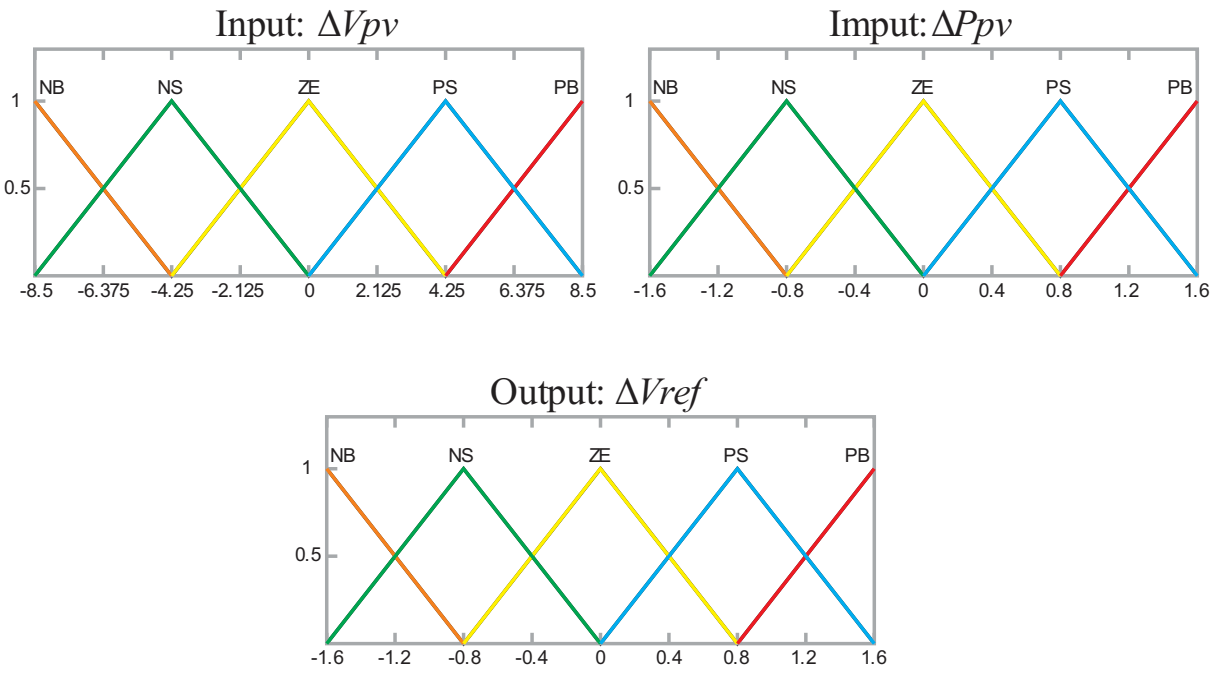

Figure 4.12: Triangular association functions.

ΔP_{pv} \ ΔV_{pv}	NB	NS	ZE	PS	PB
NB	PS	PB	NB	NB	NS
NS	PS	PS	NS	NS	NS
ZE	ZE	ZE	ZE	ZE	ZE
PS	NS	NS	PS	PS	PS
PB	NS	NB	PB	PB	PS

Figure 4.13: Rule base.

The Simulink® library has a block named Fuzzy, Figure 4.14, which allows you to insert all the settings, as shown in the window of Figure 4.15.

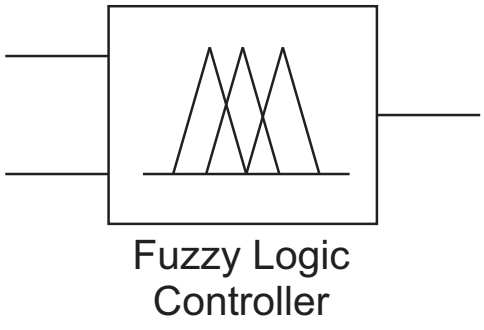

Figure 4.14: Fuzzy Matlab block.

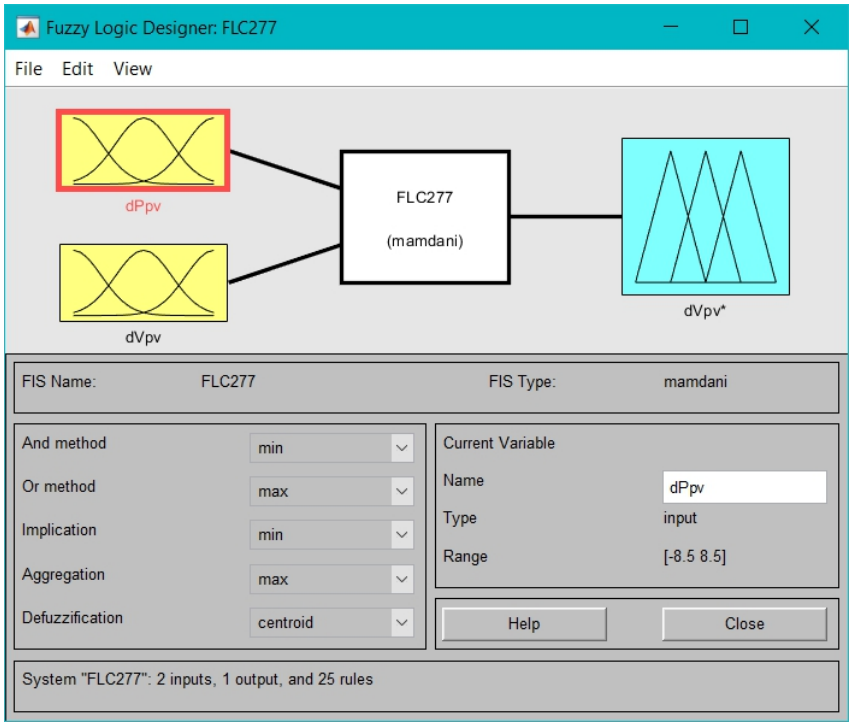

Figure 4.15: Configuration of Fuzzy Matlab block.

This block allows the implementation of the Fuzzy Logic Controller algorithm more easily. However, the block requires a lot of processing time, which prevents its use, with dSPACE 1103 working with a frequency of 10^{-3}, which was due to the activation of the IGBT's. To solve this problem the functions of triangular associations shown in Figure 4.15, were implemented as equations in a Cartesian plane, using techniques such as the integral for calculating area and center of mass. Implementing in the form of equations, it is possible to distribute the calculations in each processor clock, thus dividing the processing time and making it possible to implement it in dSPACE 1103.

4.4 Commercial PV inverters

One of the objectives of this work is to observe the MPPT algorithms of commercial inverters. This topic presents the devices available in the laboratory to perform the tests are the three inverters: Solis mini 700, Sunny Boy SB 1.5 and PIKO MP, which are shown in Figure 4.16.

(a) Solis mini 700 (b) Sunny Boy SB 1.5 (c) PIKO MP

Figure 4.16: Commercial pv inverters: (a) Solis mini 700, (b) Sunny Boy SB 1.5 e (c) PIKO MP

The main electrical characteristics of each of the inverters, for applications of MPPT algorithms, are shown in the Table 4.5.

Table 4.5: Electrical Characteristics of Commercial PV Inverters.

	Max. DC power	Max. V_{dc}	Range MPPT
Solis Mini 700	900 W	600 V	50 – 500 V
Sunny Boy SB 1.5	1.5 kW	600 V	160 – 500 V
PIKO MP	1.5 kW	450 V	75 – 360 V

Chapter 5

Experimental tests of MPPT algorithms

This chapter describes the testing process with MPPT algorithms, as well as the experimental results recently published in [22], which are obtained from the implemented set-up described in Section 4.4 and the string models discussed in Subsection 4.1.1.

The experimental tests performed are listed below:

- *Test under normal conditions* - This test evaluates the algorithms in days of clean weather, radiation and temperature almost constant, using the 5 modules Fluitecnik FTS220P;
- *Test under partial shading conditions* - This test evaluates the algorithms with panels partially shaded, using the 3 REC Solar REC275PE;
- *Test with commercial PV inverters* - This test uses 3 commercial inverters available in the laboratory, Solis mini 700, Sunny Boy SB 1.5 and PIKO MP, thus respecting the input characteristics of the devices;

5.1 Tests under normal conditions

The experimental test of the MPPT algorithms under normal conditions aims to evaluate the behavior of the MPPT techniques during clean days, in which the solar irradiation is approximately constant and only presents small variations, if observed for long periods of time.

The test uses the PV string Model A, specified in the subsection 4.1.1, composed of 5 Fluitecnik FTS220P modules. As the test is performed with the string directly converting solar radiation, the available power depends on the weather conditions to which the arrangement is exposed. To ensure reliable results, the test was carried out on a clean day and for a short

period of time, avoiding variations in irradiation and temperature. In addition, to know the available power, a functionality similar to a curve plotter was implemented, in which it would be possible to acquire the necessary part of the PV curve, to evaluate the performance in reaching the MPP of the tested algorithm.

At the beginning of the test, a voltage is imposed on pv string that grows linearly, limited from 40V to 150V, enough interval to identify the main points of the PV curve around the MPP. After acquisition, the voltage is maintained at 40V until the MPPT algorithm is started. Fixing the voltage always at the same value, 40V, all techniques always start with the same conditions. The only exception is in the Particle Swarm Optimization test, in which the control is done directly by the dutty-cycle, starting from 0.4 to 0.9, which makes the linear voltage reference decreasing. The test script is shown in Figure 5.1.

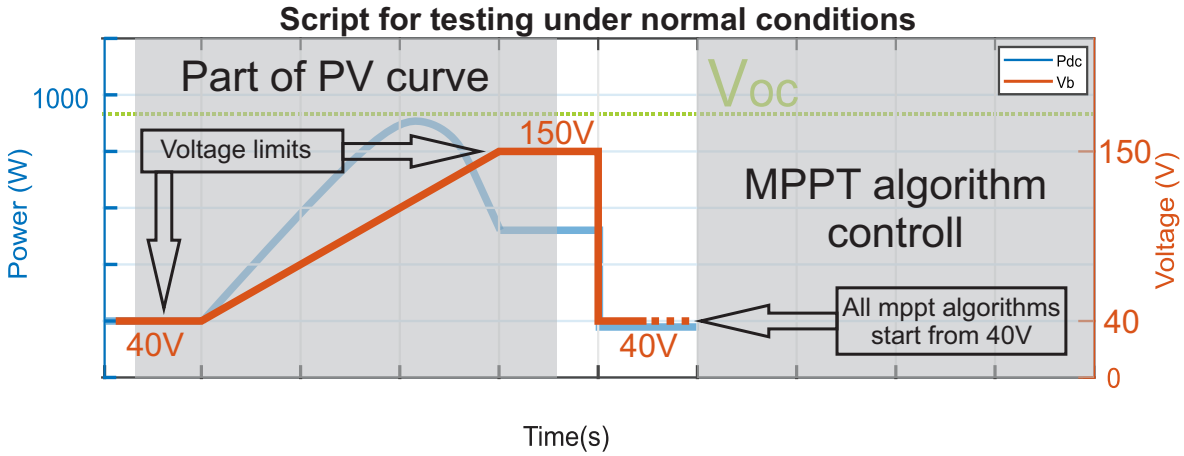

Figure 5.1: Script for testing under normal conditions.

The results of the tests under normal conditions for the P&O, IC, PSO and FLC algorithms, in the respective order, are shown in Figures 5.2 - 5.5 [22].

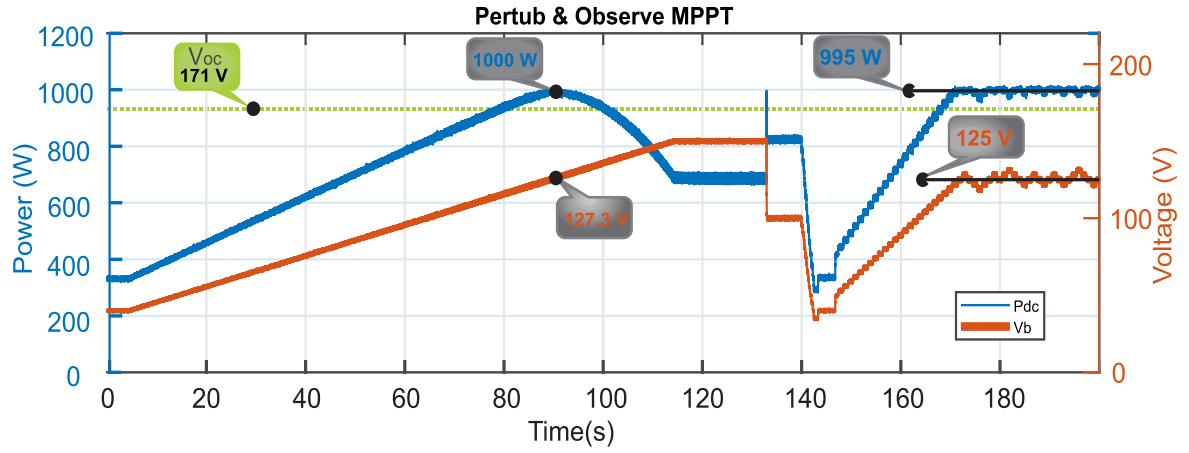

Figure 5.2: Test under normal conditions of the P&O algorithm [22].

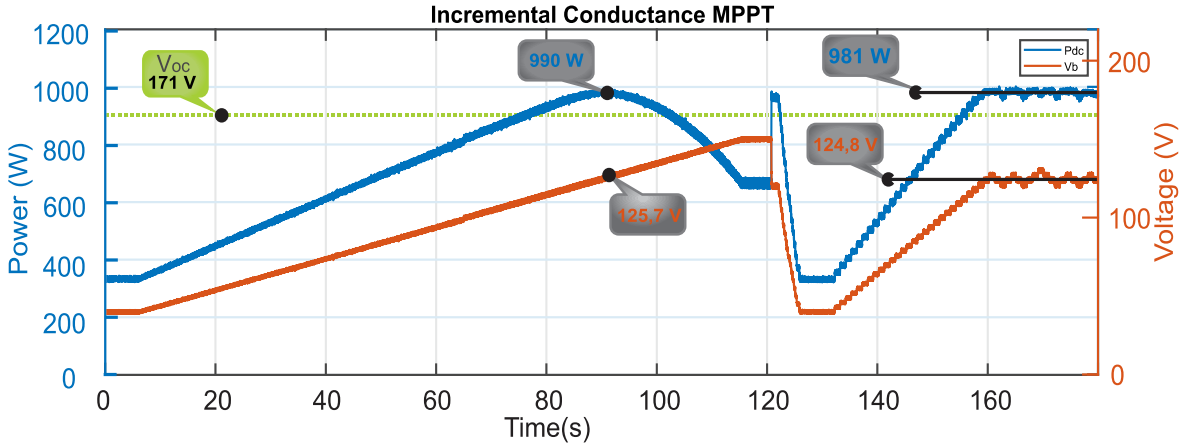

Figure 5.3: Test under normal conditions of the IC algorithm [22].

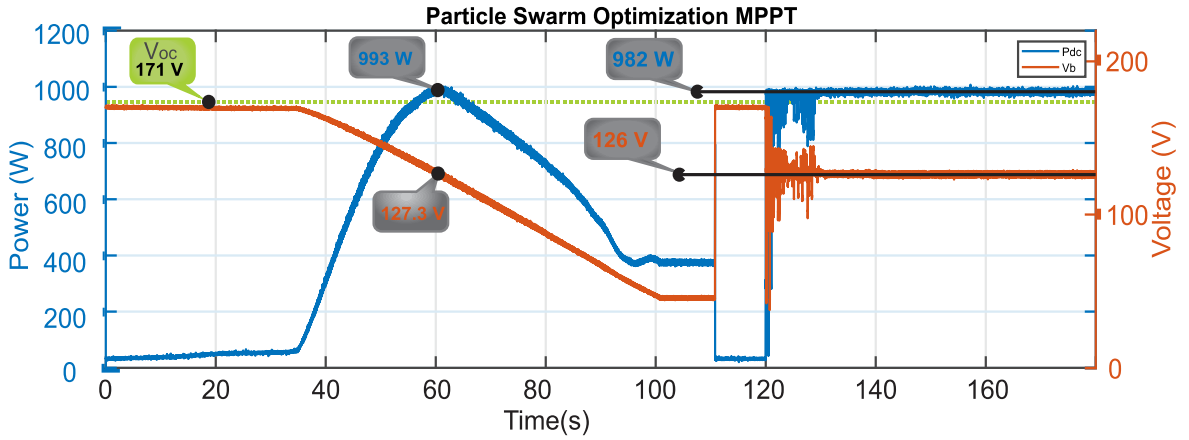

Figure 5.4: Test under normal conditions of the PSO algorithm [22].

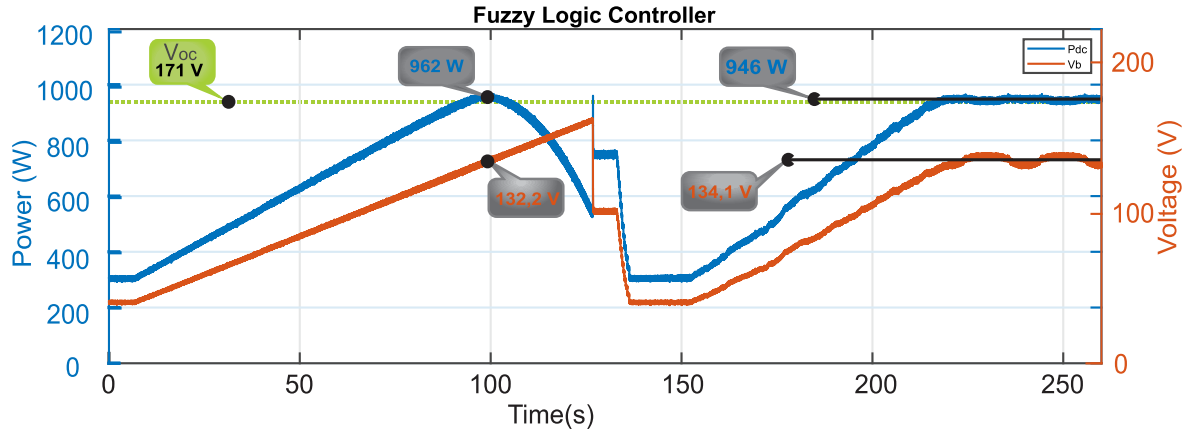

Figure 5.5: Test under normal conditions of the FLC algorithm [22].

5.2 Tests in partial shading conditions

The experimental test of MPPT algorithms in partial shading conditions aims to evaluate the performance of MPPT techniques when the radiation on the same PV module is not uniform. This can happen when something prevents the radiation from directly impacting, causing a shadow and changing the characteristics of the string.

The test uses the PV string Model B, specified in the subsection 4.1.1, composed of 3 REC Solar REC275PE PV modules. As the test is performed with the string directly converting solar radiation, the available power depends on the weather conditions to which the arrangement is exposed. To ensure reliable results, the test was performed on a clean day, for a short period of time and manually shading part of a PV module according to the needs of the test. To measure the available power, and the shape of the PV curve, as well as the 5.1 section, a feature similar to a curve plotter was implemented, where it would be possible to acquire the necessary part of the PV curve, to evaluate the performance in reaching the MPP of the tested algorithm.

At the beginning of the test, a voltage is imposed on the PV string that grows linearly, from 40V to 100V, enough interval to acquire the main points of the PV curve. After the acquisition, the voltage is maintained at 40V and only then the MPPT algorithm is started, setting the voltage always at the same value, 40V. All techniques always start with the same conditions, the only exception is in the test with Particle Swarm Optimization algorithm, in which the control is done directly by the dutty-cycle, going from 0.4 to 0.9, which makes the reference in

linear tension decreasing.

The results of the tests in partial shading conditions for the P&O, IC, PSO and FLC algorithms, in the respective order, are shown in Figures 5.6 - 5.9 [22].

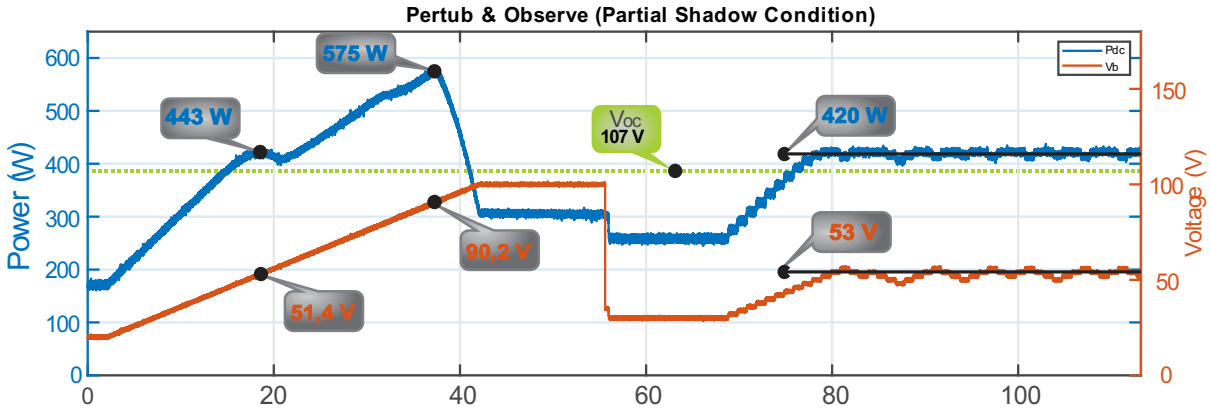

Figure 5.6: Test under shading conditions of the FLC algorithm [22].

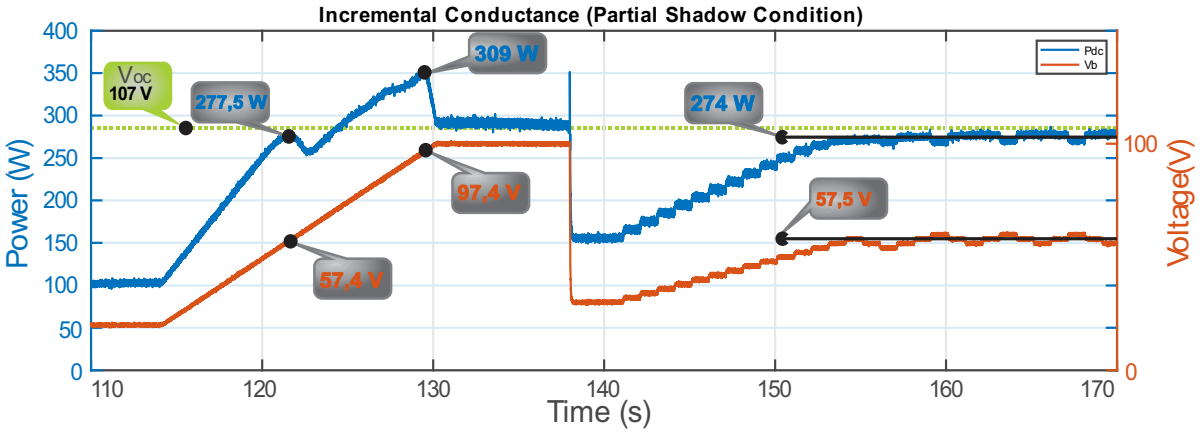

Figure 5.7: Test under shading conditions of the FLC algorithm [22].

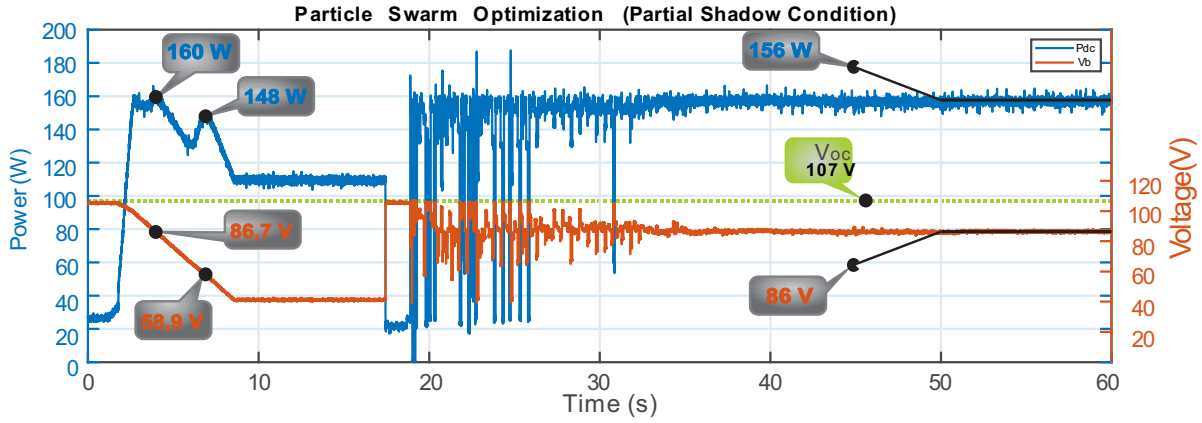

Figure 5.8: Test under shading conditions of the FLC algorithm [22].

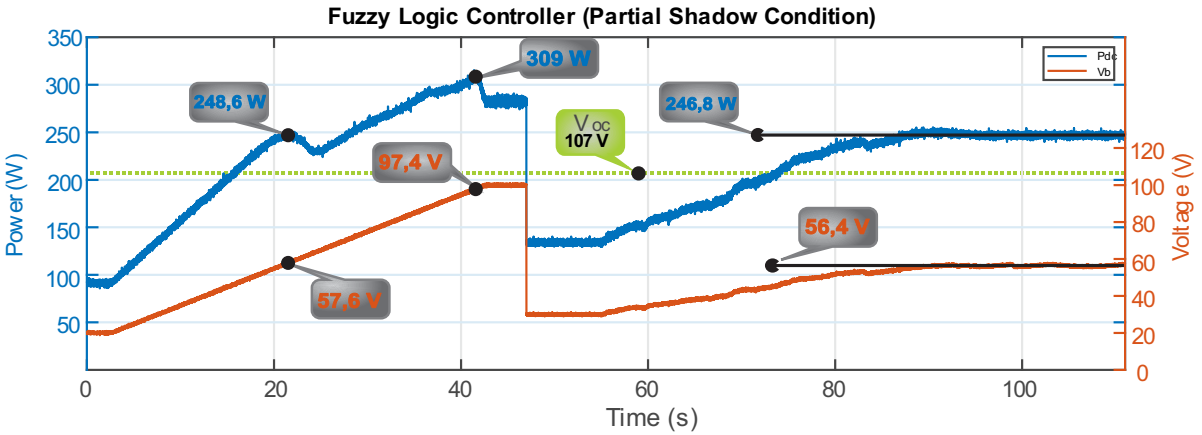

Figure 5.9: Test under shading conditions of the FLC algorithm [22].

5.3 Tests with commercial inverters

There is a difficulty in finding experimental results on the MPPT algorithms of commercial inverters. Thus, the need arose to perform this test, which aims to identify characteristics such as the operation and initialization of the algorithms and to verify the possibility of using other sources of power, such as pico-hydro generators.

For the tests, inverters available in laboratories of different prices and faricantes are used. The inverters used are shown in the section 4.4. The experiment consists of a conventional connection of a photovoltaic system, as can be seen in Figure5.10, with a set of modules connected to an inverter, which is connected to the electrical grid. During this process, it is expected that the device imposes a given voltage or current on the panel so that the maximum

power is extracted, and with the values of these quantities it is possible to observe the behavior of the algorithm. To acquire voltage or current signals, the measurement module was used with the dSPACE board panel.

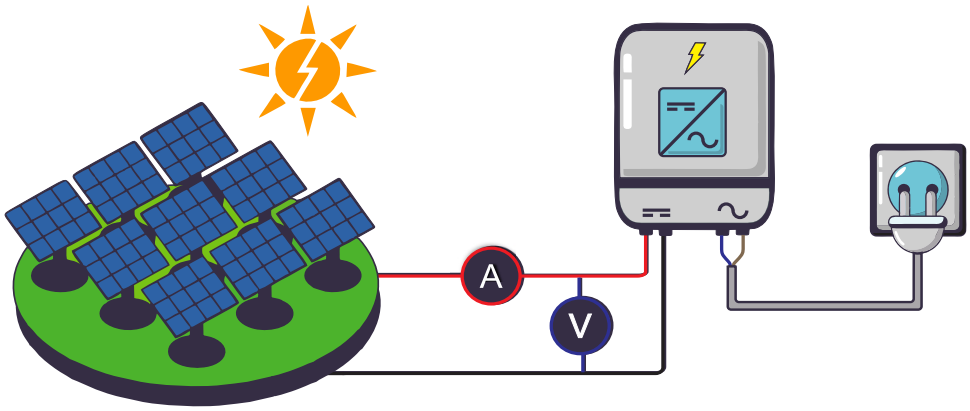

Figure 5.10: Connection between PV modules, inverter and mains to acquire voltage and current signals.

It is expected that the dynamics of the algorithm will not change with the value of the power extracted from the PV string, thus, it is not necessary to guarantee the same irradiance and temperature conditions for tests with different devices, as long as their input limits are respected.

According to availability of equipment in the laboratory, the test was carried out with the Solis mini 700, Sunny Boy SB 1.5 and Piko MP plus inverters.

During the tests with the Solis mini 700 inverter, voltage, current, and mathematically, with the product of these two, the power signal, were acquired for 150 seconds. The result is shown in Figure 5.11, with a difference in scale between the signs so, that the changes in the values are more visible.

A PV module is not a linear source, so if we vary the voltage linearly, the current will not behave similarly, and the same conclusion is valid to the contrary. By analyzing the Figure 5.11, it is observed that the voltage curve, whenever it decreases or increases, is in small steps and has a linear behavior, which indicates that the inverter operates with an MPPT algorithm similar to Pertub & Observe, with voltage control.

The test starts without the connection of the photovoltaic panels to the inverter input, which after a few seconds, is carried out, resulting in an almost instantaneous increase in

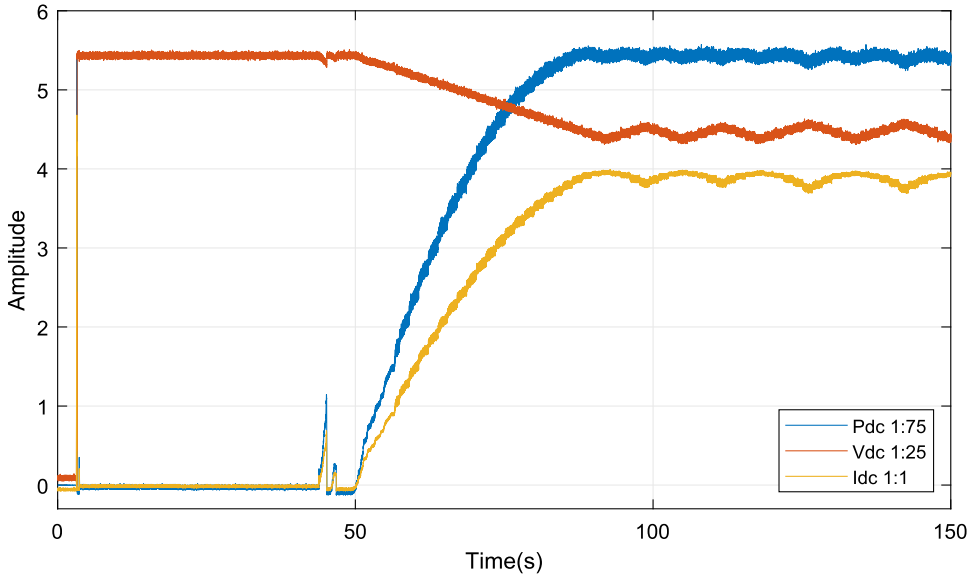

Figure 5.11: Voltage, current and power of the photovoltaic panels connected to the input of the Solis mini 700 inverter during the test.

the voltage value, equaling the open circuit voltage of the panels, as shown in Figure 5.12, obtained by limiting the graph of Figure 5.11 to the first few seconds. Acquiring this entire process avoids losing information about the device's initial behavior.

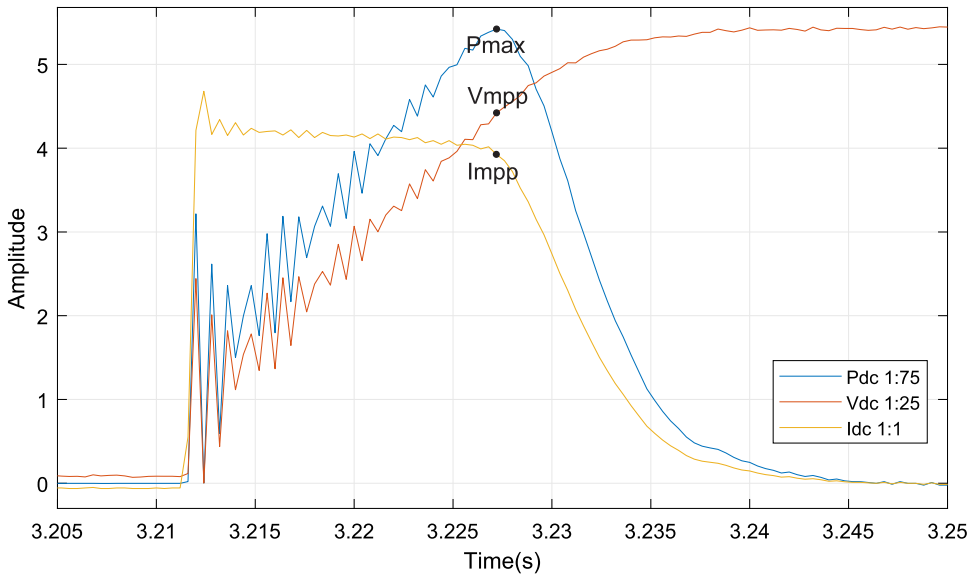

Figure 5.12: Voltage and current behavior during charging of the Solis Mini 700 input capacitor.

At the instant when DC voltage appears at the inverter input, as shown in Figure 5.12, there is a current peak that indicates the input capacitor charging. In the initial instant, with

the capacitor discharged, the maximum value corresponds to the short-circuit current and as this current tends to zero, the voltage tends to its maximum value, which corresponds to the open circuit voltage of the PV panels. In this way, the voltage and current were obtained as with an I-V curve plotter, which allows an estimate of the maximum available power and the voltage and current value corresponding to that point of operation. However, the interval is very short and it is difficult for the inverter to extract this information reliably in order to use it in its operation.

Other information obtained with the test is observed during the start of the inverter operation, after 40 seconds, as can be seen in Figure 5.13, the inverter starts from the open circuit voltage and, with fixed voltage and constant voltage increment, the algorithm tracks for the maximum power point.

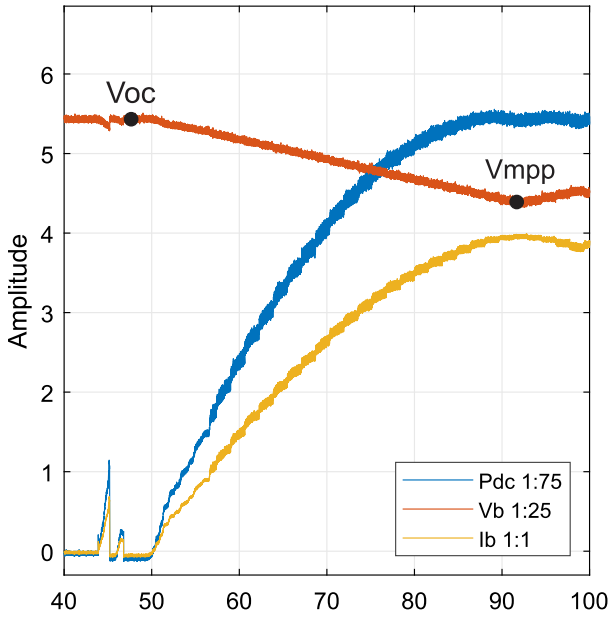

Figure 5.13: Start of operation of the inverter and search for the maximum power point using the Solis Mini 700 algorithm.

In order to check the interval of execution of the algorithm and the voltage increase/decrease, an amplification of the signals already in steady state is shown in Figure 5.14, with power oscillating around the maximum point. As can be seen in Figure 5.14, the voltage has increments of approximately 1V every 2 seconds. In addition, the decision to increase voltage (positive or negative) for the next step is made based on the power variation of the previous

step, as indicated by the arrows in Figure 5.14.

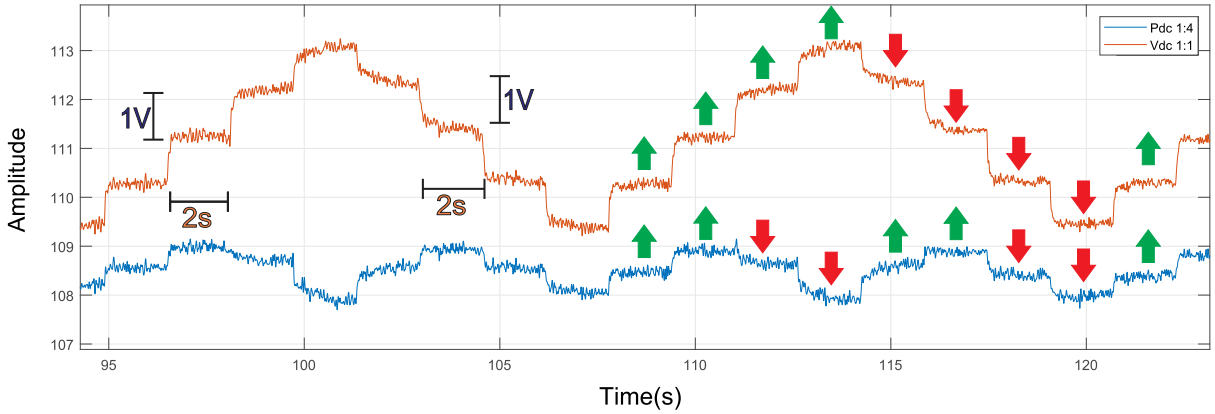

Figure 5.14: Magnification of the signals in steady state with power oscillating around the maximum point of the Solis Mini 700.

The second model is the Sunny Boy SB1.5 inverter. During the tests, voltage, current and mathematically acquired signals for 120 seconds, with the product of these two, the power signal. The result is shown in Figure 5.15, with a difference in scale between the signs, so that the changes in the values are more noticeable.

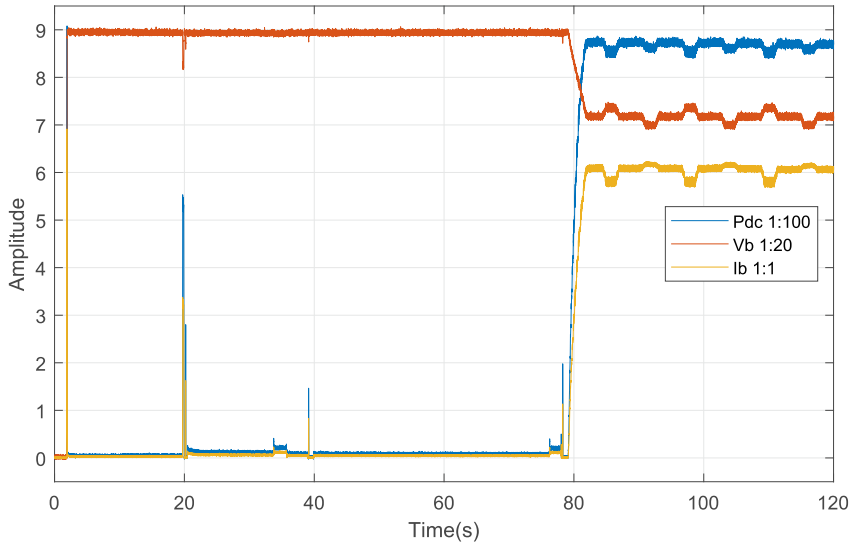

Figure 5.15: Voltage, current and power of the photovoltaic module connected to the input of the Sunny Boy SB1.5 inverter during the test.

As the PV cell is not a linear source, looking at Figure 5.15, it is noted that the voltage curve, whenever it decreases or grows, is in small steps and has a linear behavior, as in the

model above, which indicates that the inverter operates with an MPPT algorithm similar to disturbing and observing with voltage control. The test starts without connecting the photovoltaic panels to the inverter input, which, after a few seconds is made, resulting in an almost instantaneous increase in the voltage value, equaling the open circuit voltage of the string, as shown in Figure 5.16, obtained by limiting the graphic of Figure 5.15 to the first few seconds.

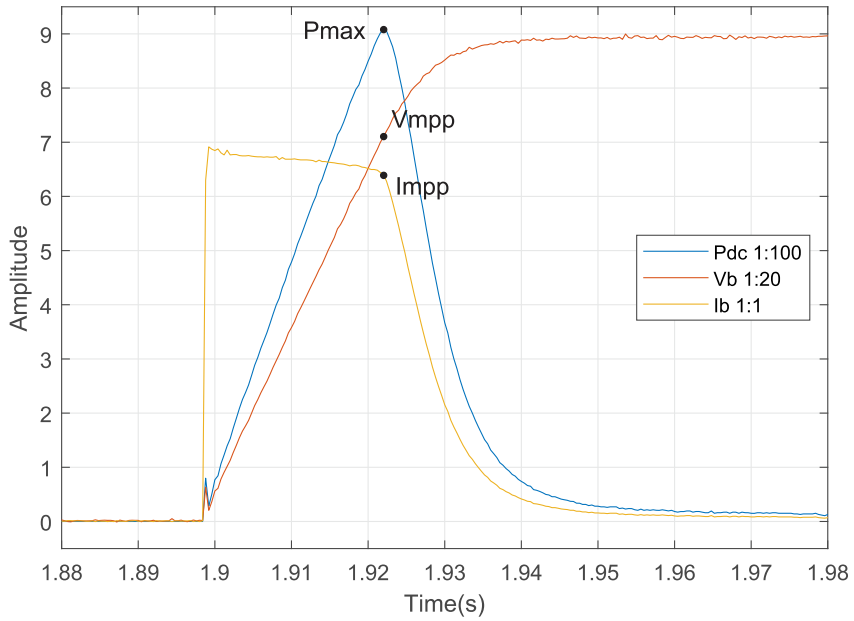

Figure 5.16: Start of the inverter operation and search for the maximum power point using the Sunny Boy SB1.5 algorithm.

At the instant when DC voltage appears at the inverter input, as can be seen in Figure 5.16, there is a current peak that indicates the charging of the input capacitor and, as in the previous test, the voltage and current has a behavior similar to that of an IV curve. Another relevant information occurs during the start of the inverter operation. After 78 seconds, as can be seen in Figure 5.17, the inverter starts from the open circuit voltage and, with fixed cadence and increment of constant voltage o, algorithm searches for the maximum power point.

In order to check the step of execution of the algorithm and the voltage increase/decrease, an enlargement of the signals, already in steady state, with approximately constant power is shown in Figure 5.18. As can be seen in Figure 5.16, the voltage has increments of approximately 3.5 V, which last for 2 seconds and are performed every 4 seconds. The voltage increase

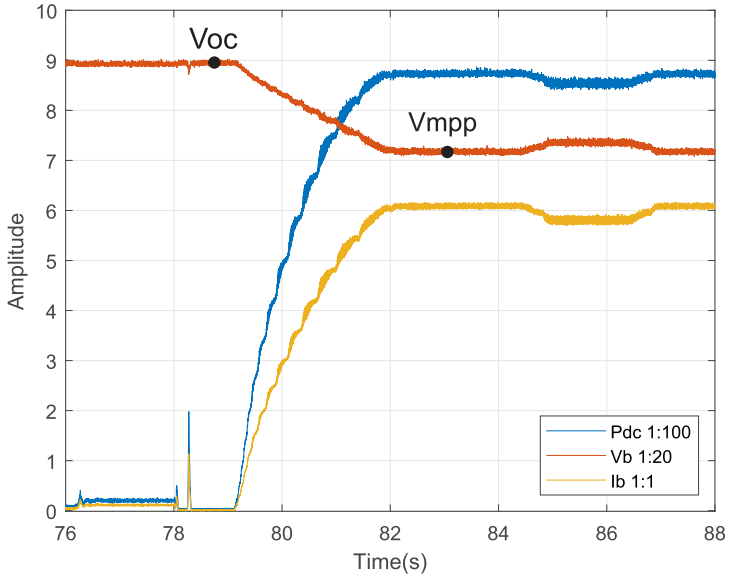

Figure 5.17: Voltage and current behavior when charging the Sunny Boy SB1.5 input capacitor.

(positive or negative) of the next step is taken based on the power variation, as indicated by the arrows in Figure 5.18.

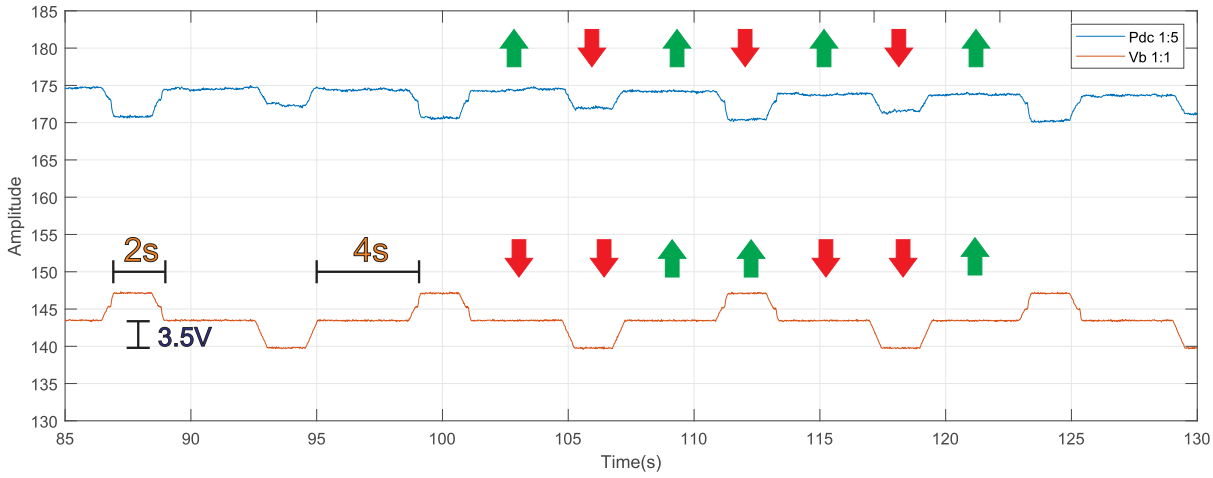

Figure 5.18: Zoom of the signals in steady state with power oscillating around the maximum point of the Sunny Boy SB1.5.

During the tests with the third model, the PIKO MP inverter, voltage, current and, mathematically, the power of these two signals was acquired for 200 seconds. The result is shown in Figure 5.19, with a difference in scale between the signs, so that the changes in the values are more noticeable.

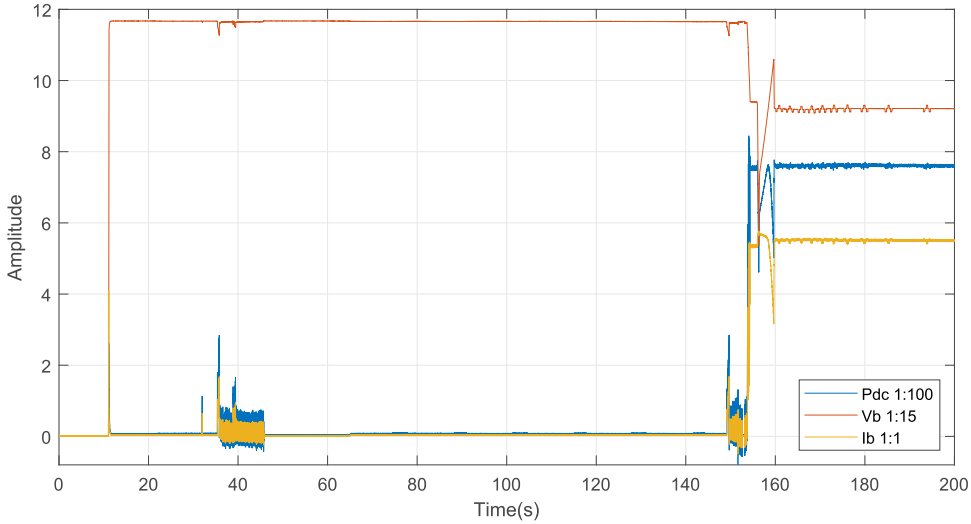

Figure 5.19: Voltage, current and power of the photovoltaic modules connected to the PIKO MP inverter input during the test.

The test starts without the connection of the PV string to the inverter input, which, after a few seconds, is performed, resulting in an almost instantaneous increase in the voltage value, equaling the open circuit voltage of the string, as shown in Figure 5.20, obtained by limiting the graph in Figure 5.19 to the first few seconds.

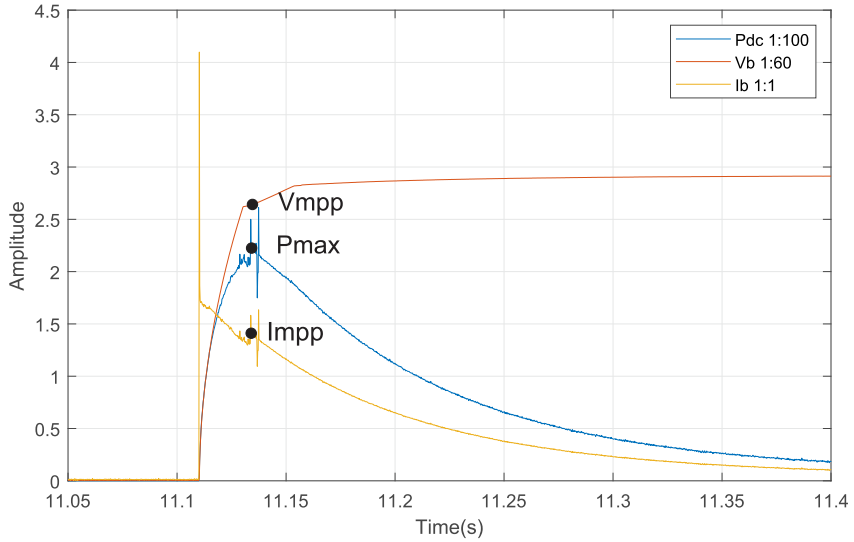

Figure 5.20: Voltage and current behavior when charging the PIKO MP input capacitor.

At the moment when DC voltage appears at the inverter input, as can be seen in Figure 5.20, there is a current peak that indicates the input capacitor charging and, as in the previous tests, the voltage and current has a behavior similar to that of an IV curve. A PV cell is not a linear source, and, through the analysis of Figure 5.21, it is observed that the voltage curve, whenever it decreases or increases, is in small steps and has a linear behavior, which indicates the inverter to operate with an MPPT algorithm similar to Pertub & Observe with voltage control. Other information regarding the test, obtained during the start of operation of the inverter, after 153 seconds, as shown in Figure 5.21. During the first moments of operation, it is possible to observe a linear voltage variation to obtain a signal similar to the IV curve of a photovoltaic module, with these data it is possible to more accurately determine the point of maximum power, which can be used by the equipment as reference for the operation of the MPPT algorithm. This process of obtaining a signal similar to the I-V curve at the start of operation is a particular feature of this model of inverter.

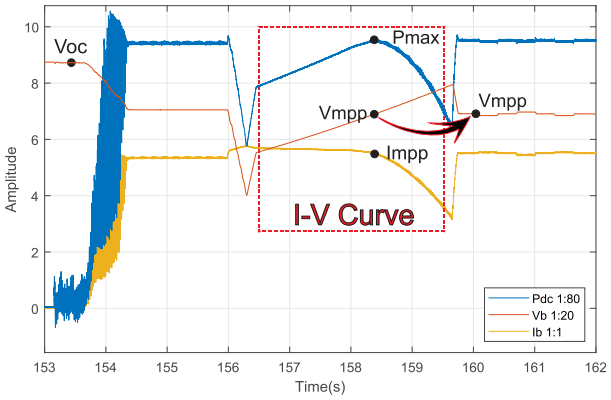

Figure 5.21: Start of operation of the inverter and search for the maximum power point using the PIKO MP algorithm.

In contrast to the MPPT algorithms of the inverters tested previously, in which the disturbance step is the same used for the increment, the PIKO MP inverter has two distinct steps. The disturbance step is made up of 3 other small steps of 3.5 V every 0.3 s, as shown in Figure 5.22. During these steps, if there is no increase in the power signal, wait a time, Δt, until the next disturbance is performed. The signals obtained during the tests show no pattern for choosing the value Δt defined by the inverter. It is only noticed that this interval increases if an increase in power is not observed during the disturbance.

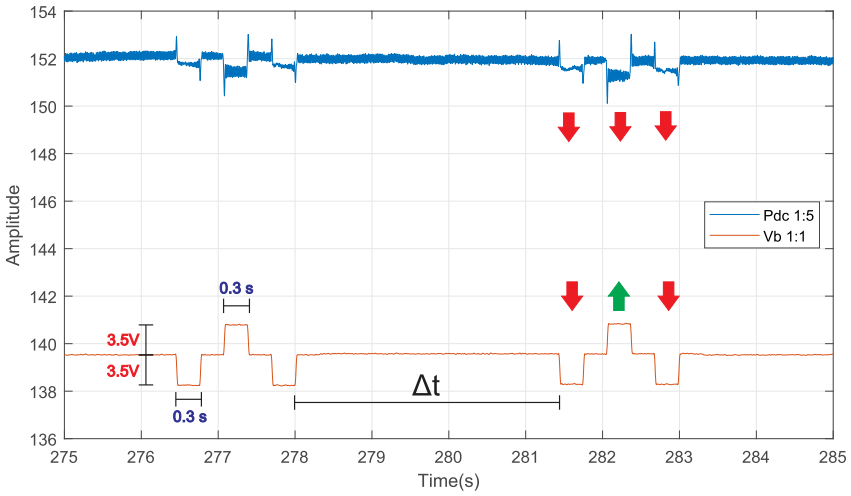

Figure 5.22: Zoom the signals in steady state with power oscillating around the maximum point of the Sunny Boy SB1.5.

As seen in Figure 5.23, after a disturbance step that verifies a voltage value for which the extracted power is greater than the current operating point, the step of ΔV increment is used, changing the inverter operating voltage value.

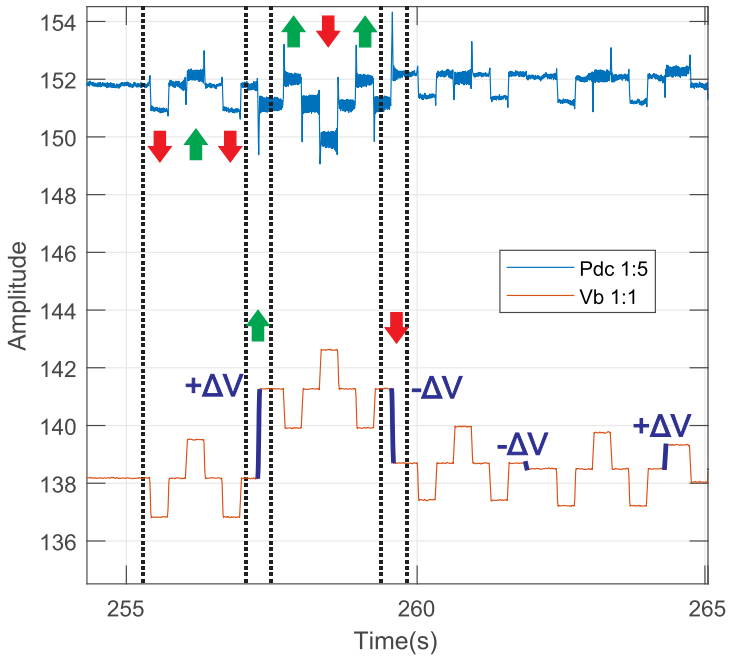

Figure 5.23: Voltage dynamics in PIKO MP.

Chapter 6

Analysis and Discussion

With the tests performed in Chapter 5, it is possible to carry out a comparative analysis between the implemented algorithms, since all tests guarantee minimally equal conditions for each of the techniques.

6.1 Ability to achieve the MPP

There is a single point of operation of the PV string, which corresponds to the point of maximum power (MPP). Tracking this point and operating as close as possible is one of the main objectives of using MPPT algorithms. However, tracking and staying in exactly that point is not a simple task, as the MPP undergoes changes with variations in weather conditions. However, the closer the operating point is to the MPP, the greater the energy extracted from the PV string.

During the tests with each of the implemented MPPT techniques, part of the PV curve is acquired, thus providing information on the PV string, such as voltage and power in the MPP. This process performed before the initialization of each MPPT algorithm, can be used to measure how close to the MPP each technique can operate and, consequently, its precision in extracting the available power from the PV string.

With the test results shown in the section 5.1, it is possible to calculate the percentage precision of the algorithm, using the equation 6.1, where V_{MPP} is the voltage in the MPP of the PV curve and V_{MPPT} is the point at which the algorithm operates.

$$Precision = 100 * \left(1 - \left(\frac{V_{MPP} - V_{MPPT}}{V_{MPP}}\right)\right) \tag{6.1}$$

Using the test results shown in the section 5.1, and using the equation 6.1, the precision

values shown in Table 6.1, which depend on the voltage in the MPP (V_{MPP}) and the point at which the algorithm operates (V_{MPPT}).

Table 6.1: Precision of MPPT Techniques.

MPPT Algorithm	P&O	IC	PSO	FLC
Precision of the MPPT	98,2%	99,3%	99,0%	98,6%

6.2 Oscillation around the MPP

The oscillation around the MPP influences the efficiency of the MPPT algorithm. Greater oscillations mean a greater loss in power extraction from the PV string. Therefore, in an analysis of MPPT techniques, it is important to measure this oscillation.

With the results of the tests shown in the section 5.1 it is possible to measure this oscillation, approximating the voltage and power curves when the MPPT algorithm reaches the MPP. The graphics in Figures 6.1 to 6.4, are enlarged parts of the graphics in Figures 5.2 to 5.5, which allows you to view and calculate the oscillations of each technique during the tests. With the test data shown in the 5.1 section, it is possible to calculate the percentage precision of the algorithm, using the equation 6.1, where V_{MPP} is the voltage in the MPP of the PV curve and V_{MPPT} is the point at which the algorithm operates.

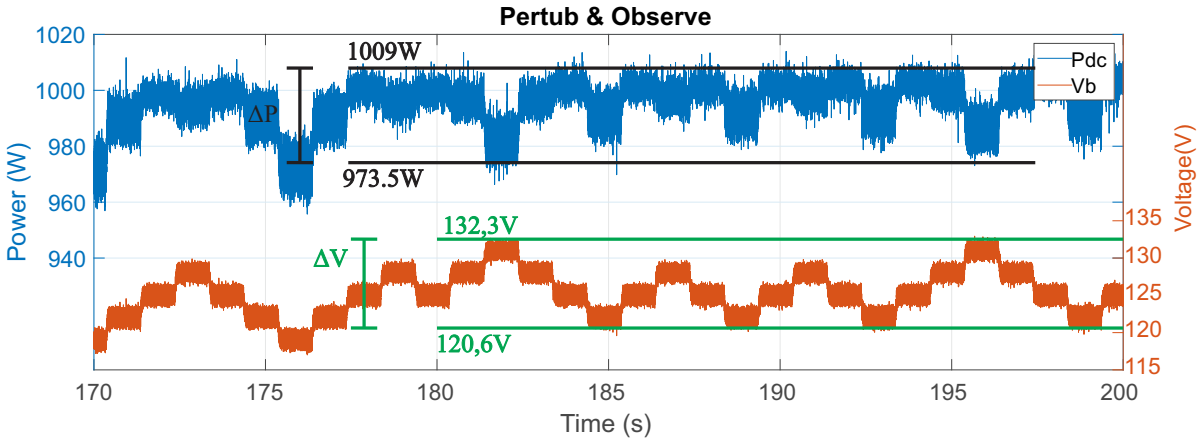

Figure 6.1: Oscillation of the P&O algorithm in MPP.

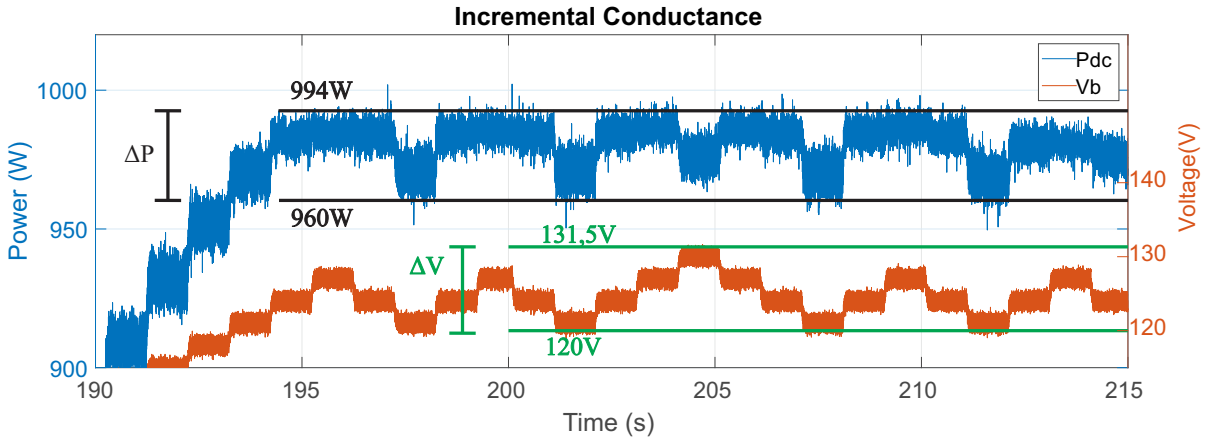

Figure 6.2: Oscillation of the IC algorithm in MPP.

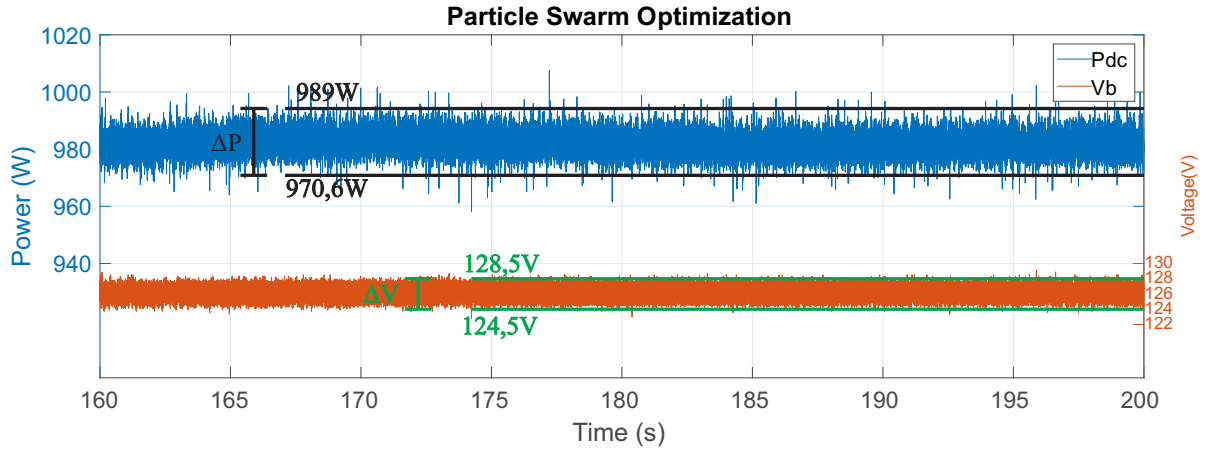

Figure 6.3: Oscillation of the PSO algorithm in MPP.

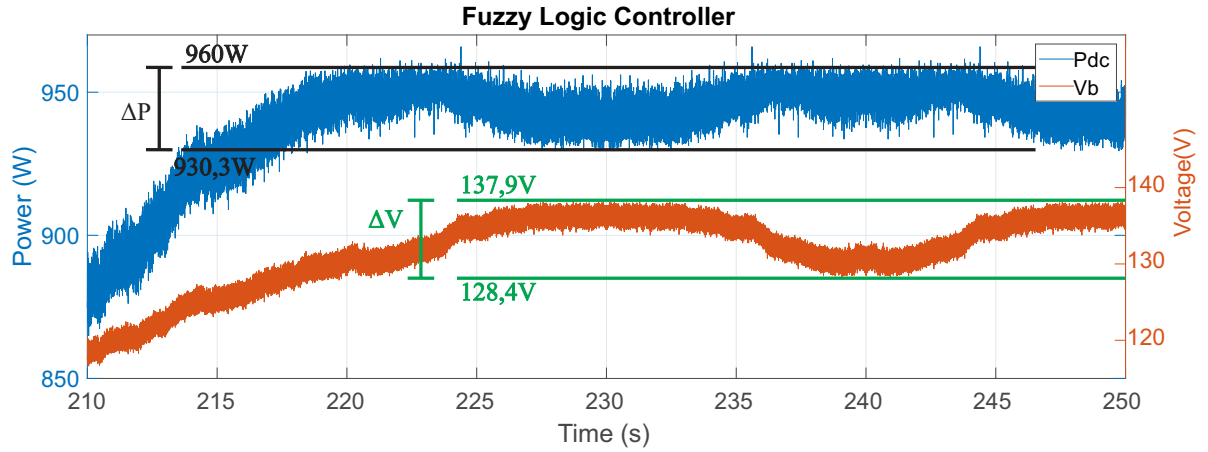

Figure 6.4: Oscillation of the FLC algorithm in MPP.

With the results shown in the graphs of Figures 5.2 to 5.5 and using the equations 6.2 and 6.3, we obtain the values shown in the table 6.1.

$$\Delta P = 100 * \left(\frac{\Delta P_{up} - \Delta P_{down}}{2 * \Delta P_{down}} \right) \tag{6.2}$$

$$\Delta V = 100 * \left(\frac{\Delta V_{up} - \Delta V_{down}}{2 * \Delta V_{down}} \right) \tag{6.3}$$

Table 6.2: Oscillation in MPP.

MPPT Algorithm	P&O	IC	PSO	FLC
ΔP%	1,82%	1,77%	0,95%	1,6%
ΔV%	4,85%	4,793%	1,61%	3,70%

6.3 Evaluation of commercial inverter algorithms

The tests with the commercial inverters shown in the section 5.3, do not aim to evaluate the accuracy and efficiency of the MPPT algorithms of the tested devices, since we cannot say with certainty which technique is actually implemented in each inverter .

The three equipments tested have MPPT techniques similar to the P&O algorithm, which can be easily observed by the voltage signal in stair shape and with well-defined values during repeated times. This could be explained by ease of implementation, which requires few calculation operations, and robustness of the technique. In addition, features such as pitch and disturbance frequency would be defined according to the range of the input voltage.

However, the preference for simplicity and robustness using the simplest techniques, under conditions of partial shading or quick changes in radiation, there may be a loss of power.

Chapter 7

Conclusion

This work presented a comparative analysis of the performance of four MPPT algorithms: Perturb & Observe, Incremental Conductance, Fuzzy Logic Controller and Particle Swarm Optimization.

The analysis is based on tests carried out experimentally under real conditions with an inverter connected to the grid. The experimental results were presented and discussed in this dissertation, and published at the 9th International Conference on Renewable Energy Research and Applications [22].

The performance of each algorithm was evaluated by means of a PV system connected to the single-phase electrical grid, consisting of a Boost converter and a full-bridge inverter.

The effectiveness of the algorithms was assessed using experimental results, taking into account two test conditions: tests under normal conditions, PV string with uniform solar irradiance and tests under partial shading, with part of the PV string covered.

In addition, tests were performed with commercial inverters available in the laboratory, which allowed us to understand the operation and initialization of the MPPT algorithms and to verify the possibility of using other sources of power, such as pico-hydro generators.

References

[1] IRENA.(2019c), *Renewable Power Generation Costs in 2019*. (visited on Jun. 20, 2020).

[2] IEA.(2020), *Renewable Power*. [Online]. Available: https://www.iea.org/reports/renewable-power (visited on Jun. 20, 2020).

[3] IRENA.(2019b), *Solar Energy*. [Online]. Available: https://www.irena.org/solar (visited on Jun. 20, 2020).

[4] IRENA.(2019d), *Solar Energy Data*. [Online]. Available: https://www.irena.org/Statistics (visited on Jun. 19, 2020).

[5] S. P. Europe, *Global Market Outlook For Solar Power (2019-2023)*. [Online]. Available: https://www.solarpowereurope.org/global-market-outlook-2019-2023/ (visited on Jun. 19, 2020).

[6] M. N. Dehedkar and S. Vitthalrao Murkute, "Optimization of pv system using distributed mppt control," in *2018 International Conference on System Modeling Advancement in Research Trends (SMART)*, 2018, pp. 216–220.

[7] A. Zekry, A. Shaker, and M. Salem, "Chapter 1 - solar cells and arrays: Principles, analysis, and design," in *Advances in Renewable Energies and Power Technologies*, I. Yahyaoui, Ed., Elsevier, 2018, ISBN: 978-0-12-812959-3. DOI: https://doi.org/10.1016/B978-0-12-812959-3.00001-0.

[8] N. Femia, G. Petrone, G. Spagnuolo, and M. Vitelli, *Power Electronics and Control Techniques for Maximum Energy Harvesting in Photovoltaic Systems*, ser. Industrial Electronics. CRC Press, 2017, ISBN: 9781351832427.

[9] W. Xiao, *Photovoltaic Power System: Modeling, Design, and Control*. Wiley, 2017, ISBN: 9781119280347.

[10] R. Teodorescu, M. Liserre, and P. Rodriguez, *Grid Converters for Photovoltaic and Wind Power Systems*, ser. Wiley - IEEE. Wiley, 2010, ISBN: 9780470667040.

[11] D. Rekioua and E. Matagne, *Optimization of Photovoltaic Power Systems: Modelization, Simulation and Control*, ser. Green Energy and Technology. Springer London, 2012, ISBN: 9781447124030.

[12] M. Kamran, M. Mudassar, M. R. Fazal, M. U. Asghar, M. Bilal, and R. Asghar, "Implementation of improved perturb & observe mppt technique with confined search space for standalone photovoltaic system," *Journal of King Saud University - Engineering Sciences*, 2018, ISSN: 1018-3639. DOI: https://doi.org/10.1016/j.jksues.2018.04.006. [Online]. Available: http://www.sciencedirect.com/science/article/pii/S101836391730380X.

[13] X.-S. Yang, *Engineering optimization : an introduction with metaheuristic applications*. Hoboken, N.J. : John Wiley, 2010.

[14] K. E. Parsopoulos and M. N. Vrahatis, *Particle Swarm Optimization and Intelligence: Advances and Applications*. Hershey, PA: Information Science Reference - Imprint of: IGI Publishing, 2010, ISBN: 1615206663.

[15] A. Kumar, P. Chaudhary, and M. Rizwan, "Development of fuzzy logic based mppt controller for pv system at varying meteorological parameters," in *2015 Annual IEEE India Conference (INDICON)*, 2015, pp. 1–6. DOI: 10.1109/INDICON.2015.7443203.

[16] M. Adly, H. El-Sherif, and M. Ibrahim, "Maximum power point tracker for a pv cell using a fuzzy agent adapted by the fractional open circuit voltage technique," in *2011 IEEE International Conference on Fuzzy Systems (FUZZ-IEEE 2011)*, 2011, pp. 1918–1922. DOI: 10.1109/FUZZY.2011.6007697.

[17] Vinod, R. Kumar, and S. Singh, "Solar photovoltaic modeling and simulation: As a renewable energy solution," *Energy Reports*, vol. 4, pp. 701 –712, 2018, ISSN: 2352-4847. DOI: https://doi.org/10.1016/j.egyr.2018.09.008. [Online]. Available: http://www.sciencedirect.com/science/article/pii/S2352484718300842.

[18] D. Sera, R. Teodorescu, and P. Rodriguez, "Pv panel model based on datasheet values," in *2007 IEEE International Symposium on Industrial Electronics*, 2007, pp. 2392–2396.

[19] G. Petrone, C. Ramos-Paja, and G. Spagnuolo, *Photovoltaic Sources Modeling*. John Wiley & Sons, Incorporated, 2017, ISBN: 9781118755877. [Online]. Available: https://books.google.com.br/books?id=_oiLAQAACAAJ.

[20] A. Pradhan and B. Panda, "A simplified design and modeling of boost converter for photovoltaic sytem," *International Journal of Electrical and Computer Engineering*, vol. 8, pp. 141–149, Feb. 2018. DOI: 10.11591/ijece.v8i1.pp141-149.

[21] K. Ang, G. Chong, and Y. Li, "Pid control system analysis, design, and technology," *Control Systems Technology, IEEE Transactions on*, vol. 13, pp. 559 –576, Aug. 2005. DOI: 10.1109/TCST.2005.847331.

[22] T. F. Guimarães and V. Leite, "Analyses of mppt algorithms in real test conditions," in *2020 9th International Conference on Renewable Energy Research and Application (ICRERA)*, 2020, pp. 164–169. DOI: 10.1109/ICRERA49962.2020.9242873.

Appendix A

Article

Title: Analyses of MPPT Algorithms in Real Test Conditions.

Published in: 2020 9th International Conference on Renewable Energy Research and Application (ICRERA).

Date of Conference: 27-30 September 2020.

Conference Location: Glasgow, United Kingdom, United Kingdom.

Analyses of MPPT algorithms in real test conditions

Thiago Fialho Guimarães
Universidade Tecnológica Federal do Paraná
Curitiba, Brazil
thiagofialho.vg@gmail.com

Vicente Leite
Research Centre in Digitalization and Intelligent Robotics (CeDRI)
Polytechnic Institute of Bragança
Bragança, Portugal
avtl@ipb.pt

***Abstract*—Maximum Power Point Tracking (MPPT) algorithms are of major importance for optimized yield in grid-connected PV systems. Many algorithms have been investigated. However, most of the works compare these algorithms based on a literature review or on simulation. This paper presents an experimental analysis of MPPT techniques: two of the simplest (Perturb & Observe and Incremental Conductance) and two of the most complex (Fuzzy Logic Controller and Particle Swarm Optimization). The results are carried out in real test conditions, with and without shadow. The power converter is based on a boost converter and a voltage source inverter. The control is implemented using Simulink® and dSPACE 1103 real-time controller board. Moreover, the MPPT techniques of three commercial string inverters are also analysed.**

Keywords— MPPT, Perturb & Observe, Incremental Conductance, Fuzzy Logic Controller, Particle Swarm Optimization.

I. INTRODUCTION

The two biggest difficulties in the generation of photovoltaic (PV) systems are the low conversion efficiency of the electric potential and the high cost of PV cells [1]. However, meteorological conditions must be considered, since PV cells have non-linear I-V characteristics, which change with variation in radiation, temperature and load [2]. Due to these characteristics, the maximum power point (MPP) changes constantly and is not known. However, it can be found through search algorithms.

A maximum power point tracking algorithm (MPPT) aims to keep the PV modules operating in the MPP, regardless of the load and weather variations [3]. A MPPT algorithm improves the annual yield of every PV string or module. Extensive research has been done during last decade. Dozens of algorithms have been investigated [4, 5], from the simplest ones [6] to the most complex [7, 8]. Many studies are dedicated to comparative analysis. With a few exceptions [9], most are based on a review of previous works [4, 7] or, at most, on simulation [6, 10]. Some previous works are not conclusive about the benefits of intelligent algorithms compared to the simplest ones, considering their drawbacks [7]. This work compares two well-known MPPT algorithms, Perturb & Observe (P&O) and Incremental Conductance (IC), with two intelligent algorithms, Fuzzy Logic Controller (FLC) and Particle Swarm Optimization (PSO). This comparison is based on experimental analysis. Furthermore, three commercial PV inverters, from different manufacturers, are also analyzed regarding their MMPT algorithms.

II. OVERVIEW OF MPPT TECHNIQUES

In general, MPPT algorithms work by combining load impedance with source impedance, thus finding MPP and transferring maximum power. This technique consists of controlling a DC-DC converter to perform the impedance matching [11].

Among the MPPT algorithms proposed in the literature, this work evaluates the performance of four techniques that are among the most discussed, such as Perturb & Observe, Incremental Conductance, Fuzzy Logic Controller and Particle Swarm Optimization. The choice of these algorithms allows the analysis of techniques with different types of approaches and levels of complexity under the same test conditions.

A. Perturb & Observe

The MPPT Perturb and Observe (P&O) algorithm is one of the simplest and most discussed techniques in the literature [1]. This technique applies a small disturbance to the system in order to follow the path that leads to the MPP.

In the flowchart of Fig. 1 it is possible to observe the steps of the MPPT P&O algorithm. The first steps are to read the voltage and current and to calculate the power of the PV string. After the acquisition of the signals, at time t_k, the power and voltage values are compared with the respective previous samples, at t_{k-1}, and based on this information the path to the MPP is chosen [12].

When there is an increase or decrease in voltage, thus imposing a small disturbance, the operating point of the PV string changes and, consequently, the extracted power [12]. If this power change is positive, the algorithm continues to increase the voltage, but if the power change is negative, it indicates that the MPP is in the opposite direction, so the algorithm starts to reduce the voltage to reach the MPP. In this way, part of the P-V curve is covered by small constant steps, that is, by small disturbances to find the MPP.

In this case, as shown in the flow chart of Fig. 1, the disturbance is made every second, being controlled by the voltage with a 3 V step (ΔV). The choice of these values is made according to the voltage range.

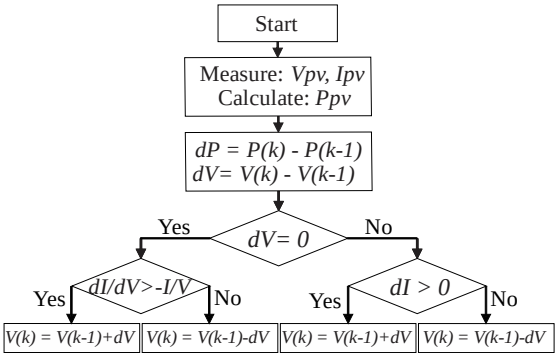

Fig. 1. Flowchart of MPPT P&O algorithm.

XXX-X-XXXX-XXXX-X/XX/$XX.00 ©20XX IEEE

B. *Incremental Condutance*

The MPPT Incremental Conductance (IC) algorithm, like P&O, applies a small disturbance to the system to follow the path that leads to the MPP [1]. What differentiates the two techniques are the parameters used for decision, which in the IC algorithm are conductance (1) and incremental conductance (2).

$$GG = I_{pv}/V_{pv} \tag{1}$$

$$\Delta GG = \Delta I_{pv}/\Delta V_{pv} \tag{2}$$

The decision to increase or decrease the voltage is made based on (1) and (2). Let us take as an example a P-V or P-I characteristic curve of a PV string. When the operating point is on the left of the MPP, the value of the derivative of the curve assumes a negative value. On the contrary, if it is on the right of the MPP, the derivative takes on a positive value. When working on the MPP, it takes on a zero value, as shown in (3).

$$\begin{cases} \Delta GG = -GG, & \text{in MPP} \\ \Delta GG > -GG, & \text{on the left} \\ \Delta GG < -GG, & \text{on the right} \end{cases} \tag{3}$$

The algorithm compares the conductance and the incremental conductance to decide when to increase or decrease the PV voltage to track the MPP, as shown in the flow chart of Fig. 2. In this case, the disturbance is done at every second, being controlled by the voltage, with a 3 V step (ΔV). These values are chosen according to the voltage range.

C. *Particle Swarm Optimization*

Particle Swarm Optimization (PSO) is a technique that uses stochastic variables based on a population for solving optimization problems [13].

The PSO algorithm was not designed for applications in PV systems. However, it can be adapted for this new purpose. This technique works by researching the space of a function, adjusting the position of each particle [14]. In a PV application, it boils down to adjust the duty cycle of the DC-DC converter for each particle at a point on the P-V curve. At the end of each cycle, the position of each particle is adjusted by a speed factor given by (4) and the result is given by (5).

$$v_i(t+1) = w v_i(t) + c_1 R_1 (p_{bi}(t) - d_i(t)) + c_2 R_2 (G_b(t) - d_i(t)) \tag{4}$$

$$d_i(t+1) = d_i(t) + v_i(t+1) \tag{5}$$

Where v_i is the velocity of particle i, c_1 and c_2 are the acceleration constants, w is the weight of inertia, R_1 and R_2 are random values between 0 and 1, p_{bi} is the location with the best fitness of all the visited location of particle i, d_i is the position of particle i, and G_b is the best position found.

With the flowchart shown in Fig. 3, it is possible to observe the steps of the PSO algorithm in each iteration of the process. This was the PSO algorithm implemented in this work. Four particles and a delay of 100 ms are used for each iteration. The values of the constants used in (4) were $w=0.4$, $c_1=1.2$ and $c_2=2$.

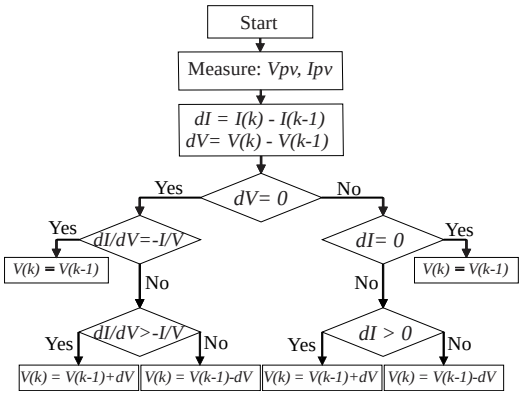

Fig. 2. Flowchart of MPPT IC algorithm.

D. *Fuzzy Logic controll*

The Fuzzy Logic Control (FLC) algorithm, as shown in Fig. 4, generally consists of three stages: fuzzification, rule base and defuzzification [11]. During fuzzification, the numeric input variables are converted to linguistic variables based on a membership function [11]. Generally, the inputs for a diffuse logic MPPT controller are voltage variation ΔV_{pv} (6) and power variation ΔP_{pv} (7).

$$\Delta V_{pv} = V_{pv}(t) - V_{pv}(t-1) \tag{6}$$

$$\Delta P_{pv} = \Delta V_{pv} \times \Delta I_{pv} \tag{7}$$

In this work, in the fuzzification stage, five triangular association functions were used for the inputs and output. The two input variables were converted to linguistic values: Negative Big (NB), Negative Small (NS), Zero (ZE), Positive Small (PS), and Positive Big (PB). The membership functions of inputs and the output are shown in Fig. 5.

Mamdani's method is used for fuzzy inference. For defuzzification, the centroid method was used to calculate the ΔV_{ref} output. The rule base used to find the output is shown in the table of Fig. 5, where the reference voltage for the PI controller (V_{ref}) is calculated based on (8).

$$V_{ref} = V_{pv} + \Delta V_{ref} \tag{8}$$

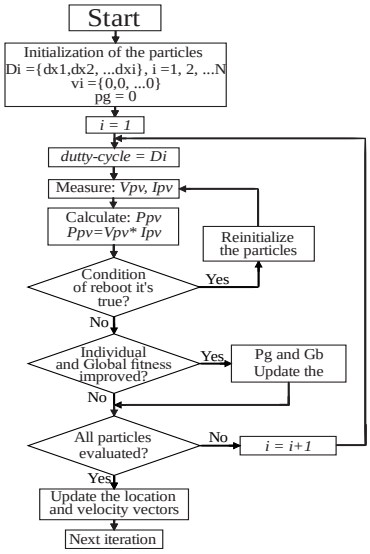

Fig. 3. Flowchart of MPPT FLC algorithm.

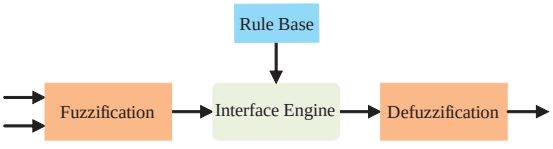

Fig. 4. Flowchart of MPPT FLC algorithm.

In the defuzzification stage, the fuzzy logic controller output is converted to a controller variable. In this case, it is the voltage reference (V_{ref}) used in a PI controller. Fuzzy logic controllers can work with inaccurate inputs, not needing a precise linear mathematical model, but with a high implementation cost.

III. Experimental Plataform

For testing the MPPT algorithms, the PV inverter topology shown in Fig. 6 was used. The power topology has a bidirectional DC-DC converter, configured as a boost converter, followed by a voltage source inverter.

For the control of the boost converter, the MPPT algorithm gives the input voltage reference to PI controller or directly the duty cycle. This imposes the dc output voltage of the PV string. The voltage source inverter controls the power by controlling the dc-link voltage, maintaining the voltage on the DC bus at 400V, higher than the peak voltage of the grid. The control of the current injected into the grid is based on voltage-oriented control [15, 16].

A. *Experimental set-up*

The power structure, shown in Fig.7, is based on the Powerex PM75RLA120 intelligent power module, with a 3-phase IGBT voltage source inverter. A leg is used for the boost converter, where one of the IGBTs always remains off, functioning as a diode, while the other semiconductor is controlled by the MPPT algorithm. The remaining two legs are used as a single-phase voltage source inverter, which is controlled by voltage-oriented control.

The MPPT algorithms and the voltage oriented control were implemented in Simulink®. Then, dSPACE 1103 real-time controller board and ControlDesk® application were used for the real-time control.

B. *PV Strings*

For the tests, two PV strings were used, shown in Fig. 8, which are formed by PV modules of different number and model. For tests under normal conditions, two strings A and B were used. The first is composed by 5 Fluitecnik FTS220P modules. The second, is composed by 3 REC Solar REC275PE modules and was used in tests with partial shading.

The individual characteristics of the two PV modules used are shown in Table I. Both models have 60 PV cells and a bypass diode every 20 cells.

TABLE I. Characteristics of Photovoltaic Models

PV modules of	*Max. Power*	I_{SC}	V_{OC}	I_{MPP}	V_{MPP}
String A	220 W	8.30 A	36.76 V	7.51 A	29.38 V
String B	275 W	9.25 A	38.70 V	8.74 A	31.50 V

The MPPT algorithms are evaluated in different situations: tests under normal conditions and tests with partial shading.

The tests under normal conditions were carried on clean days. During these tests the irradiation does not suffer sudden changes, and the same happens with the P-V curve of the PV string, which has only a MPP, as shown by the blue curves of Fig. 9. These are the normal conditions for the operation of a PV system.

The tests in partial shading conditions evaluate MPPT algorithms when there is shadow on part of the PV string surface. Therefore, the irradiation is not the same in all cells, and the module is under partial shading. Thus, the curve may have more than one maximum, which makes the work of the algorithms more difficult, since only one of these maximums is the MPP. An example of partial shading, in a generic way, is illustrated by the red curves of Fig. 9.

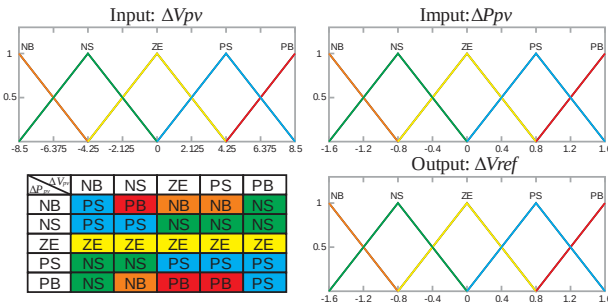

Fig. 5. Membership functions.

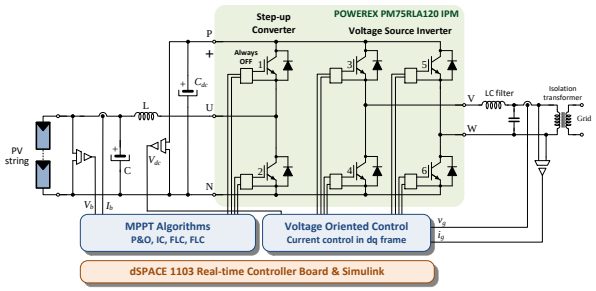

Fig. 6. Power topology.

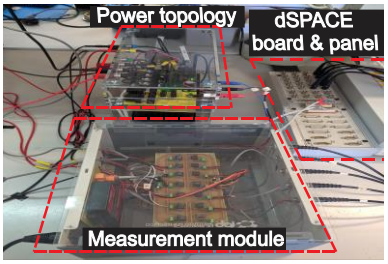

Fig. 7. Experimental set-up.

Fig. 8. String A (at left) and string B (at right).

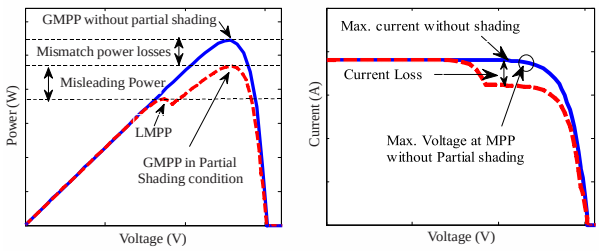

Fig. 9. Generic PV curves: P-V (on the left) and I-V (on the right).

IV. Experimental Results

The experimental results are divided into three groups, according to tests under normal conditions, tests with partial shading and tests with commercial inverters. During each test, the performance of each algorithm is verified individually.

A. Tests Under Normal Conditions

During clean days, irradiation does not suffer sudden changes. The same happens with the PV curve of the PV arrangement, remaining almost constant and with only a maximum, as shown in the blue curves of Fig. 9. These are the normal operating conditions expected for a PV system.

Tests under normal conditions (with string A) evaluate the algorithms in a clean day, with radiation and temperature almost constant during the test. The results are shown in Fig. 10 to Fig. 13. At the beginning, a P-V curve is traced. Thus, 65% of the P-V curve is acquired, around V_{MPP}, in order to identify the MPP. During this process, and with the PSO, the string output voltage is imposed by increasing the duty cycle linearly from 0.4 to 0.9. Therefore, the string output voltage decreases from a value above the MPP to a value below the MPP, as can be seen in Fig. 12. With the other algorithms, the string output voltage is linearly increased from 40V to 150V. After the acquisition of the P-V curve around MPP, the algorithms are enabled, always starting at 40V, as shown in Fig. 10, Fig. 11 and Fig. 13.

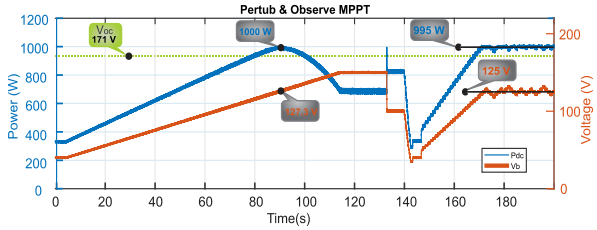

Fig. 10. Test under normal conditions of the P&O algorithm.

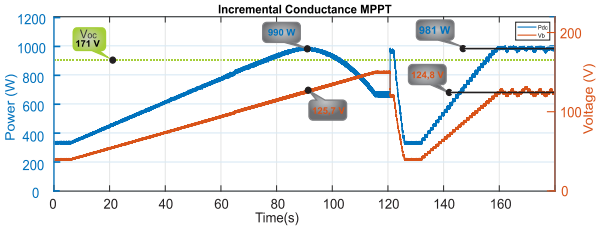

Fig. 11. Test under normal conditions of the IC algorithm.

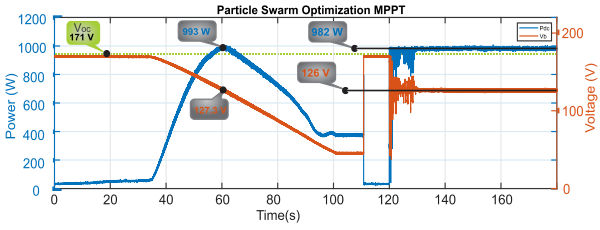

Fig. 12.Test under normal conditions of the PSO algorithm.

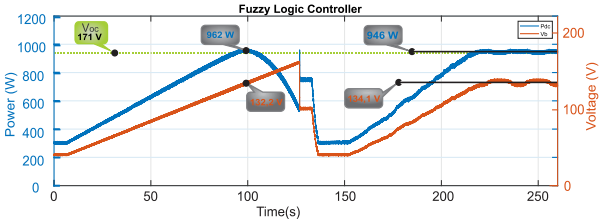

Fig. 13. Test under normal conditions of the FLC algorithm.

B. Test in partial shading conditions

This second test uses string B, because it is easier to shade part of the modules since it is on the ground in front of the laboratory. One of the three PV modules was partially shaded (as shown in Fig. 8). At the beginning, a P-V curve is traced as for tests A. After the acquisition of the P-V curve around MPP, the algorithms are enabled, always starting at 40V, as shown in Fig. 14 to Fig. 17.

C. Tests with commercial inverters

The purpose of these tests is to evaluate the MPPT algorithms of three commercial inverters available in the laboratory: Solis mini 700 with string A, and Sunny Boy SB1.5 and PIKO MP with string B. The strings were chosen according to the rated characteristics of the inverters. During this test, the photovoltaic string is connected to inverter and the dc voltage and current are acquired using the same set-up. The results, from the initialization until the steady-state operation around MPP, are shown in Fig. 18 to Fig. 20.

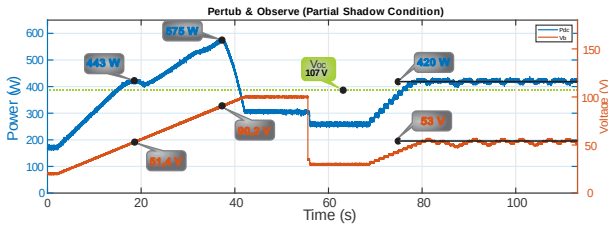

Fig. 14. Test under shading conditions of the P&O algorithm.

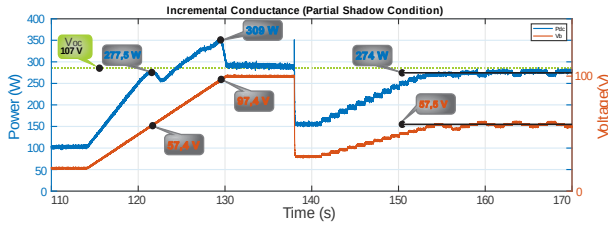

Fig. 15. Test under shading conditions of the IC algorithm.

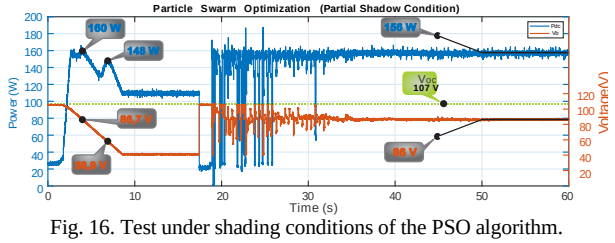

Fig. 16. Test under shading conditions of the PSO algorithm.

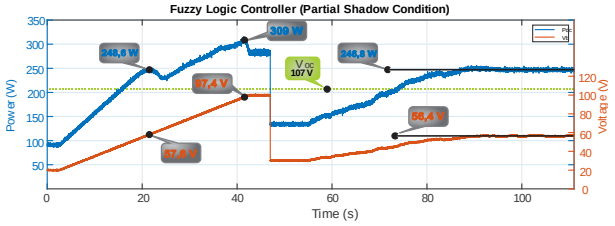

Fig. 17. Test under shading conditions of the FLC algorithm.

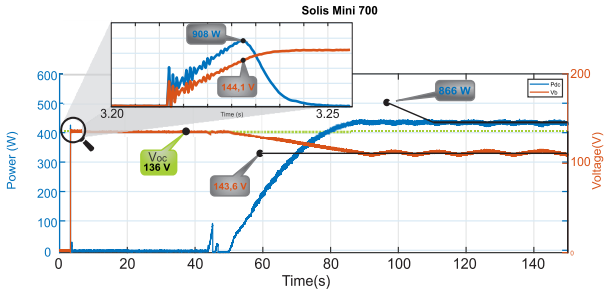

Fig. 18. Results with commercial inverter Solis Mini 700.

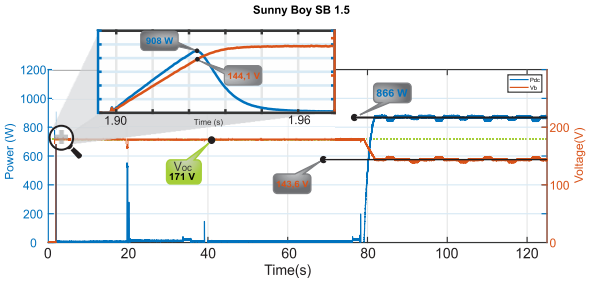

Fig. 19. Results with commercial inverter Sunny Boy SB 1.5.

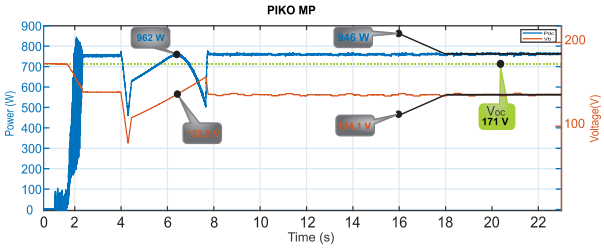

Fig. 20. Results with commercial inverter Piko MP.

V. Discussion

With the tests carried out, it is possible to compare some characteristics of the algorithms, such as precision in reaching the MPP, oscillation in the MPP and the ability to deal with partial shading problems.

A. *Ability to achieve the MPP*

There is a single point of operation of the PV string that corresponds to the MPP. For an algorithm to reach exactly that point it is not so simple. The closer to the MPP the algorithm operates, the more power is extracted from the PV string. The P-V curve drawn in the tests under normal conditions, before the initialization of each MPPT algorithm, can be used to measure how close to the MPP each technique can operating. With the test data, using (9), where V_{MPP} is the voltage at the MPP of the P-V curve and V_{MPPT} is the point at which the algorithm operates.

$$Precision = 100*(1-((V_{MPP}-V_{MPPT})/V_{MPP}) \quad (9)$$

Using (9), the values shown in Table II were found.

TABLE II. Precision of MPPT techniques

P&O	*IC*	*PSO*	*FLC*
98,2%	99,3%	99,0%	98,6%

B. *Oscillation around the MPP*

One of the factors that imply the efficiency of the algorithm is the oscillation around the MPP, as it results in loss of power. Using the test results under normal conditions it is possible to measure this oscillation. The graphs in Fig. 21 to

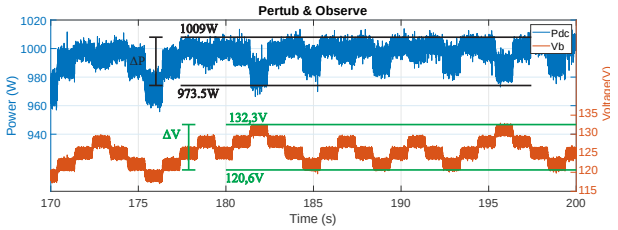

Fig. 21. Oscillation of the P&O algorithm in MPP.

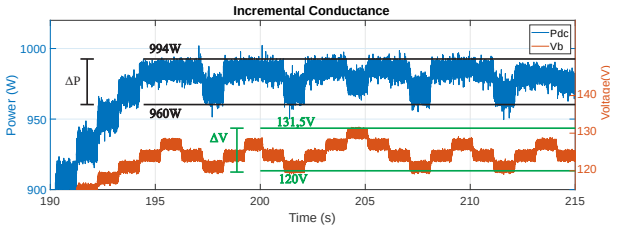

Fig. 22. Oscillation of the IC algorithm in MPP.

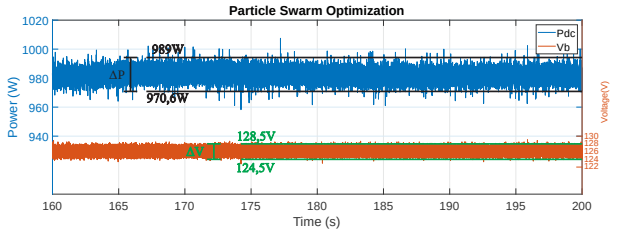

Fig. 23. Oscillation of the PSO algorithm in MPP.

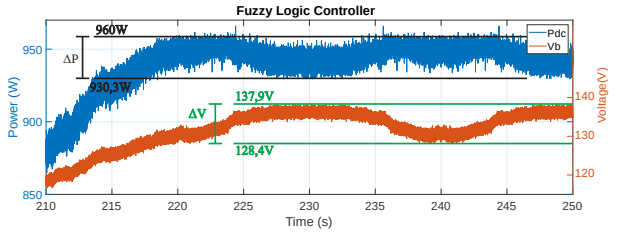

Fig. 24. Oscillation of the FLC algorithm in MPP.

Fig. 24 are a zoom of the graphs in Fig. 10 to Fig. 13 when the algorithm has already reached the MPP, which allows to know how much is the oscillation.

The values of the power and voltage oscillations of all implemented algorithms are shown in Table III.

TABLE III. Power and Voltage Oscilation in the MPP

	P&O	*IC*	*PSO*	*FLC*
ΔP	1,82%	1,77%	0,95%	1,60%
ΔV	4,85%	4,79%	1,61%	3,70%

C. *Under parcial shadow*

With the results of the tests under partial shading conditions, as can be seen in Table IV, only the PSO algorithm was able to find the GMPP, while the other algorithms reached only a local maximum.

TABLE IV. Ability of the Algorithms to Deal with Partial Shading

P&O	*IC*	*PSO*	*FLC*
No	No	Yes	No

Therefore, under partial shading conditions, P&O, IC and FLC are not able to achieve the GMPP. The PSO algorithm is

the only one of the four evaluated algorithms capable of dealing with partial shading conditions.

D. Evaluation of commercial inverter algorithms

As can be seen in the tests of commercial inverters, Fig. 18 to Fig. 20, the three tested equipment have MPPT techniques similar to the P&O algorithm. This can be explained by the ease of implementation and the robustness of the technique. Moreover, characteristics such as step and perturb frequency are defined according to the range of the input voltage.

VI. CONCLUSION

This work presents an experimental comparative analysis of four MPPT algorithms of different complexity: Perturb & Observe, Incremental Conductance, Fuzzy Logic Controller and Particle Swarm Optimization. The first two are simple and widely used and the latest two are more complex. The simplest can be implemented with less processing, but on the other hand, they lose in accuracy. The results obtained under shadow effect, with more than one point of maximum power point, show that only the PSO algorithm is able to find the true maximum power point. Tests carried out with three commercial PV inverters seem to use of simple algorithms, similar to Perturb & Observe.

REFERENCES

[1] A. K. Gupta and R. Saxena, "Review on widely-used MPPT techniques for PV applications," 2016 International Conference on Innovation and Challenges in Cyber Security (ICICCS-INBUSH), Noida, 2016, pp. 270-273, doi: 10.1109/ICICCS.2016.7542321.

[2] A. W. Leedy and K. E. Garcia, "Approximation of P-V characteristic curves for use in maximum power point tracking algorithms," 45th Southeastern Symposium on System Theory, Waco, TX, 2013, pp. 88-93, doi: 10.1109/SSST.2013.6524945.

[3] Faranda, R.; Leva, S.; Maugeri, V., "MPPT techniques for PV Systems: Energetic and cost comparison," Power and Energy Society General Meeting - Conversion and Delivery of Electrical Energy in the 21st Century, 2008 IEEE , vol., no., pp.1,6, 20-24 July 2008.

[4] Bhatnagar, Pallavee & Nema, Rajesh. (2013). Maximum Power Point Tracking Control Techniques: State-of-the-Art in Photovoltaic Applications. Renewable and Sustainable Energy Reviews. 23. 224–241. 10.1016/j.rser.2013.02.011. (Article)

[5] A. K. Podder, N. K. Roy and H. R. Pota, "MPPT methods for solar PV systems: a critical review based on tracking nature," in IET Renewable Power Generation, vol. 13, no. 10, pp. 1615-1632, 29 7 2019, doi: 10.1049/iet-rpg.2018.5946. (Article)

[6] A. K. Gupta and R. Saxena, "Review on widely-used MPPT techniques for PV applications," 2016 International Conference on Innovation and Challenges in Cyber Security (ICICCS-INBUSH), Noida, 2016, pp. 270-273, doi: 10.1109/ICICCS.2016.7542321.

[7] M. E. E. Telbany, A. Youssef and A. A. Zekry, "Intelligent Techniques for MPPT Control in Photovoltaic Systems: A Comprehensive Review," 2014 4 th International Conference on Artificial Intelligence with Applications in Engineering and Technology, Kota Kinabalu, 2014, pp. 17-22, doi: 10.1109/ICAIET.2014.13.

[8] Motahhir, Saad & Aoune, Ayoub & Abdelaziz, el ghzizal & Sebti, Souad & Derouich, Aziz. (2017). Comparison between Kalman filter and incremental conductance algorithm for optimizing photovoltaic energy. Renewables: Wind, Water, and Solar. 4. 8. 10.1186/s40807-017-0046-8.

[9] M. A. G. de Brito, L. Galotto, L. P. Sampaio, G. d. A. e Melo and C. A. Canesin, "Evaluation of the Main MPPT Techniques for Photovoltaic Applications," in IEEE Transactions on Industrial Electronics, vol. 60, no. 3, pp. 1156-1167, March 2013, doi: 10.1109/TIE.2012.2198036.

[10] V. K. Viswambaran, A. Ghani and E. Zhou, "Modelling and simulation of maximum power point tracking algorithms & review of MPPT techniques for PV applications," 2016 5 th International Conference on Electronic Devices, Systems and Applications (ICEDSA), Ras Al Khaimah, 2016, pp. 1-4, doi: 10.1109/ICEDSA.2016.7818506.

[11] D. Haji and N. Genc, "Fuzzy and P&O Based MPPT Controllers under Different Conditions," 2018 7th International Conference on Renewable Energy Research and Applications (ICRERA), Paris, 2018, pp. 649-655, doi: 10.1109/ICRERA.2018.8566943.

[12] M. Kamran, M. Mudassar, M. R. Fazal, M. U. Asghar, M. Bilal, R. Asghar, Implementation of improved Perturb & Observe MPPT technique with confined search space for standalone photovoltaic system, Journal of King Saud University - Engineering Sciences, 2018, ISSN 1018-3639, https://doi.org/10.1016/j.jksues.2018.04.006.

[13] K. Ishaque, Z. Salam, M. Amjad and S. Mekhilef, "An Improved Particle Swarm Optimization (PSO)–Based MPPT for PV With Reduced Steady-State Oscillation," in IEEE Transactions on Power Electronics, vol. 27, no. 8, pp. 3627-3638, Aug. 2012, doi: 10.1109/TPEL.2012.2185713.

[14] R. B. A. Koad, A. F. Zobaa and A. El-Shahat, "A Novel MPPT Algorithm Based on Particle Swarm Optimization for Photovoltaic Systems," in IEEE Transactions on Sustainable Energy, vol. 8, no. 2, pp. 468-476, April 2017, doi: 10.1109/TSTE.2016.2606421.

[15] V. Leite, Â. Ferreira and J. Batista, "Bidirectional vehicle-to-grid interface under a microgrid project," 2014 IEEE 15th Workshop on Control and Modeling for Power Electronics (COMPEL), Santander, 2014, pp. 1-7, doi: 10.1109/COMPEL.2014.6877175.

[16] Breve M.M., Leite V. (2020) Control of a Bidirectional Single-Phase Grid Interface for Electric Vehicles. In: Nesmachnow S., Hernández Callejo L. (eds) Smart Cities. ICSC-CITIES 2019. Communications in Computer and Information Science, vol 1152.